Photophysics of Perovskite Nano- and Microcrystals

Chen, Junsheng

2018

Document Version:
Publisher's PDF, also known as Version of record

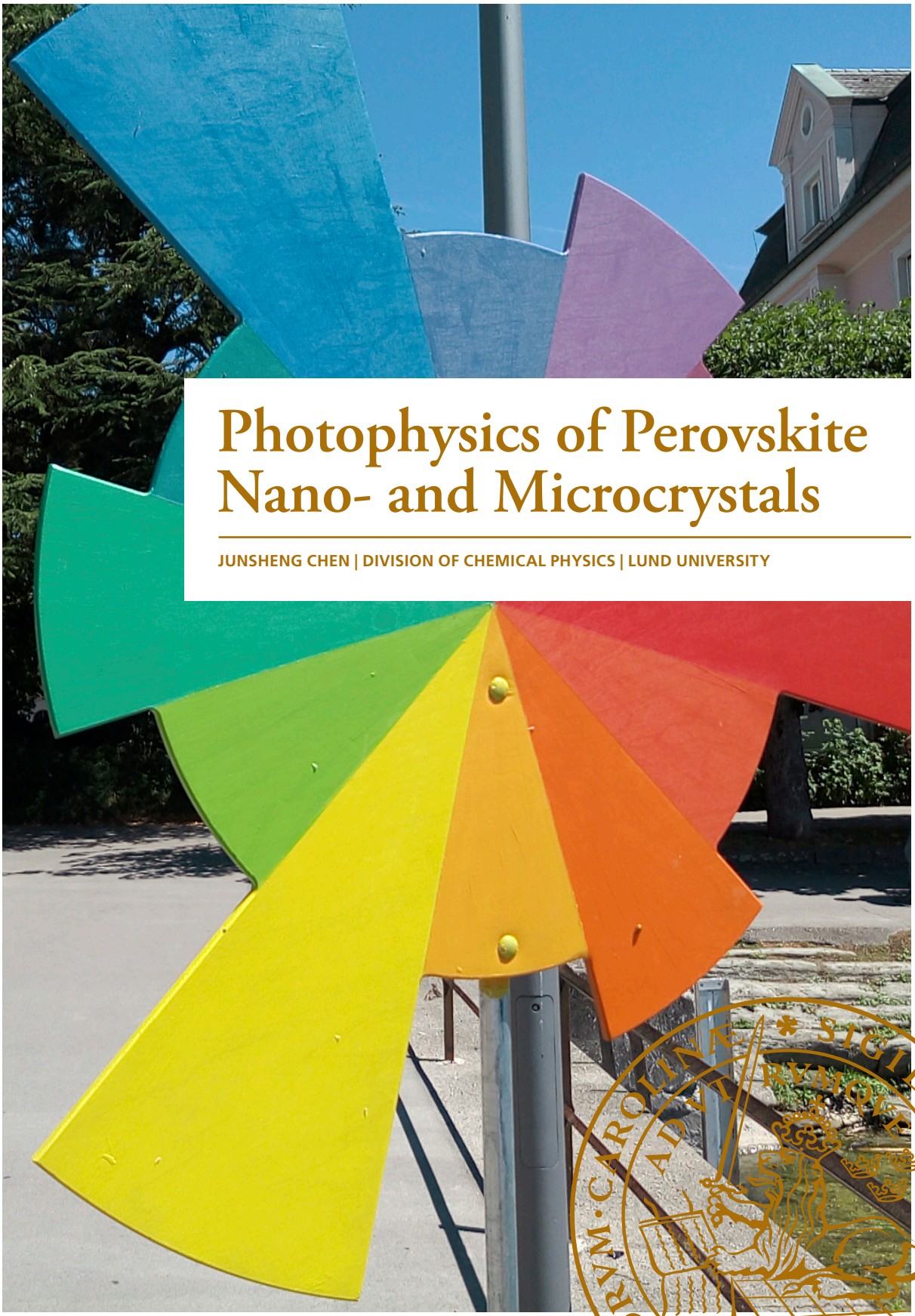

Photophysics of Perovskite Nano- and Microcrystals

JUNSHENG CHEN | DIVISION OF CHEMICAL PHYSICS | LUND UNIVERSITY

Photophysics of Perovskite Nano- and Microcrystals

Junsheng Chen

LUND
UNIVERSITY

DOCTORAL DISSERTATION
by due permission of the Faculty of Science, Lund University, Sweden.
To be defended at lecture hall F, Kemicentrum, Naturvetarvägen 16, 22362 Lund.
Friday the 16th of March at 13:15 pm.

Faculty opponent
Prof. Dr. Tianquan Lian

Organization
LUND UNIVERSITY
Division of Chemical Physics
Department of Chemistry
P.O. Box 124
SE-22100 Lund, Sweden

Author(s)
Junsheng Chen

Document name
Doctoral Dissertation

Date of issue
2018-02-20

Sponsoring organization

Title and subtitle
Photophysics of Perovskite Nano- and Microcrystals

Abstract

The demand and consumption of energy is increasing dramatically all around the world. Broad adoption of fossil fuels has triggered an enormous threat to the environment. To ensure sustainability of our species and habitat, new solutions to fulfill the energy demand have to be found. Innovative materials offer the possibility to generate scalable renewable energy, which is efficient and environmentally friendly. In recent years, it was demonstrated that lead halide perovskite (LHP) materials prepared with superior optoelectronic properties which are desirable for solar-cell applications. Moreover, the solution processing ensures cheap production of those materials. In order to optimize and widely adopt LHPs as a key component for solar energy generators, it is important to understand the fundamental photophysical processes governing their unique behavior.

In this thesis we studied the photophysics of LHP nano- (NC) and microcrystals (MC) using spectroscopic methods. We investigated the photostability of NCs, and found the light irradiation induced particle aggregation. Furthermore, we revealed large two-photon absorption cross sections of these NCs, and we conclude that the two-photon absorption process populates the exciton band through a virtual state. Moreover, we have demonstrated the crucial role of size distribution in explaining the difference between the one-photon excited and two-photon excited photoluminescence (PL).

We fabricated photodetectors using micrometer-sized LHP crystals as building blocks, which show high responsivity as well as fast response in both the visible (one-photon absorption process) and the near infrared (NIR) region (two-photon absorption process). We also elucidated the underlying mechanism for the enhanced photoresponse by efficient charge collection, low trap density and high charge carrier mobility in the MCs.

In order to develop environmentally friendly materials, we replaced the lead element with less toxic bismuth in LHP structures to form the bismuth-based perovskite NCs, which exhibit tunable PL but with low quantum yield. The photophysical studies in such NCs with time-resolved spectroscopy attributed the low PL emission intensity to a fast trapping process.

Key words: Ultrafast spectroscopy, Perovskite, Nanocrystals, Two-photon absorption, Photostability

Classification system and/or index terms (if any)

Supplementary bibliographical information

Language
English

ISSN and key title

ISBN 978-91-7422-567-9

Recipient's notes

Number of pages: 146

Price

Security classification

Photophysics of Perovskite Nano- and Microcrystals

Junsheng Chen

LUND
UNIVERSITY

Cover photo: Color wheel, which is taken by Junsheng Chen in Lindau, Germany, June 2017.

Faculty of Science
Department of Chemistry
Division of Chemical Physics

ISBN 978-91-7422-567-9 (Print)
ISSN 978-91-7422-568-6 (PDF)

Printed in Sweden by Media-Tryck, Lund University
Lund 2018

孤独不是永远独自一人，而是一颗没有希望的心

Contents

Abstract i

Popular Science Summary ii

Populärvetenskaplig sammanfattning iii

Acknowledgement v

List of Publications vii

Abbreviations ix

Chapter 1: Introduction 1

1.1 Materials for Renewable and Sustainable Energy 1

1.2 Perovskite Materials: Nanocrystals and Microcrystals, and Their Applications 2

1.2.1 The Crystal Structure of Perovskite 2

1.2.2 Perovskite Nanocrystals 3

1.2.3 Perovskite Microcrystals 6

1.3 Photophysics in Nanocrystals 6

1.3.1 Excited-State Dynamics in Nanocrystals 7

1.3.2 Two-Photon Absorption 10

Chapter 2: Experimental Methods 13

2.1 Synthesis of Perovskite Nanocrystals and Microcrystals 13

2.1.1 Synthesis of Perovskite Nanocrystals 13

2.1.2 Synthesis of Lead Halide Perovskite Microcrystals 15

2.2 Time-Resolved Photoluminescence Spectroscopy 15

2.2.1 Time-Correlated Single Photon Counting 16

2.2.2 The Streak Camera 17

2.2.3 Transient Absorption 18

2.3 Two-Photon Absorption Cross Section Measurement 20

Chapter 3: Stability of $CsPbBr_3$ Nanocrystals 23

3.1 Highly Dynamic Ligand Binding in $CsPbBr_3$ Nanocrystals 23

3.2 Photostability of $CsPbBr_3$ Nanocrystals 24

3.2.1 $CsPbBr_3$ Nanocrystals under Different Storage Conditions 24

3.2.2 Instability of $CsPbBr_3$ Nanocrystals under Light Irradiation.....25
Chapter 4: Photophysics of Two-Photon Excited $CsPbBr_3$ Nanocrystals.....29
4.1 Two-Photon Excited Photoluminescence of $CsPbBr_3$ Nanocrystals.....29
4.2 Two-Photon Absorption Process in $CsPbBr_3$ Nanocrystals.....30
4.3 Enhanced Size Selection in Two-Photon Excitation for $CsPbBr_3$ Nanocrystals.....32
4.4 Refinement of the Size-Dependent Two-Photon Absorption Cross Section.....34
Chapter 5: Lead Halide Perovskite Microcrystals for Photodetector Applications 35
5.1 Photodetectors based on Lead Halide Perovskite Microcrystals.....35
5.1.1 Photodetector Schemes based on Lead Halide Perovskite Crystals.....35
5.1.2 Basic Important Parameters of Photodetectors.....36
5.2 $CsPbBr_3$ Microcrystals for Near-Infrared Light Detection.....38
Chapter 6: Photophysics in Lead Free Caesium Bismuth Halide Perovskite Nanocrystals.....41
6.1 $Cs_3Bi_2X_9$ Nanocrystal Synthesis.....41
6.2 Photoluminescence of $Cs_3Bi_2X_9$ NCs.....42
Chapter 7: Conclusion.....45
References.....47

Abstract

The demand and consumption of energy is increasing dramatically all around the world. Broad adoption of fossil fuels has triggered an enormous threat to the environment. To ensure sustainability of our species and habitat, new solutions to fulfill the energy demand have to be found. Innovative materials offer the possibility to generate scalable renewable energy, which is efficient and environmentally friendly. In recent years, it was demonstrated that lead halide perovskite (LHP) materials prepared with superior optoelectronic properties which are desirable for solar-cell applications. Moreover, the solution processing ensures cheap production of those materials. In order to optimize and widely adopt LHPs as a key component for solar energy generators, it is important to understand the fundamental photophysical processes governing their unique behavior.

In this thesis we studied the photophysics of LHP $CsPbBr_3$ nano- (NC) and microcrystals (MC) using spectroscopic methods. We investigated the photostability of NCs, and found the light irradiation induced particle aggregation. Furthermore, we revealed large two-photon absorption cross sections of these NCs, and we conclude that the two-photon absorption process populates the exciton band through a virtual state. Moreover, we have demonstrated the crucial role of size distribution in explaining the difference between the one-photon excited and two-photon excited photoluminescence (PL).

We fabricated photodetectors using micrometer-sized $CsPbBr_3$ LHP crystals as building blocks, which show high responsivity as well as fast response in both the visible (one-photon absorption process) and the near infrared (NIR) region (two-photon absorption process). We also elucidated the underlying mechanism for the enhanced photoresponse by efficient charge collection, low trap density and high charge carrier mobility in the MCs.

In order to develop environmentally friendly materials, we replaced the lead element with less toxic bismuth in LHP structures to form the bismuth-based perovskite NCs, which exhibit tunable PL but with low quantum yield. The photophysical studies in such NCs with time-resolved spectroscopy attributed the low PL emission intensity to a fast trapping process.

Popular Science Summary

The global consumption of energy is increasing each year because of population growth and rising living standards. Earth is facing global warming, depletion of fossil fuels (i.e. coal, oil and natural gas) and increase of environmental pollution. Therefore, it is urgent to search for renewable energy sources and efficient ways of using harvested energy. High-performance materials are the key component to harvest and use energy efficiently. In recent years, lead halide perovskite materials have emerged as promising versatile materials, which would be suitable for renewable energy generation, such as solar-cells. Moreover, their nanomaterial counterpart can be used for fabricating devices for our daily life such as lighting (e.g. light emitting diodes, LEDs), displays (e.g. TVs), photodetection (e.g. cameras) and lasers. All these devices are based on the principle of light absorption or emission, in which many different photophysical processes are involved.

A comprehensive understanding of the photophysics in lead halide perovskite materials will be the key to further improve the performance of the materials and devices. In this thesis, we studied the photo-stability of lead halide perovskite nanocrystals (crystals in nanometer size, 1 nm = 10^{-9} m, i.e. about ten-thousandths of the diameter of a human hair). Lead halide perovskite nanocrystals show applicability for two-photon pumped laser applications. Thus, here, we investigated the two-photon absorption process in those lead halide perovskite nanocrystals in detail. We also utilized micrometer-sized lead halide perovskite crystals to fabricate photodetectors with high performance. Furthermore, concerning the environment, we tried to replace the toxic lead in lead halide perovskite nanocrystals with less toxic bismuth. The bismuth-based perovskite nanocrystals show tunable, but weak photoluminescence emission in the visible spectral range. By using spectroscopic methods we have identified a trapping process, which leads to such low emission intensity. Hence, it is possible to suppress the trapping process and increase the photoluminescence emission of bismuth-based perovskite NCs, and this will ensure that such NCs show high potential for LED applications.

Populärvetenskaplig sammanfattning

Varje år ökar världens energiförbrukning på grund av befolkningstillväxt och ökande levnadsstandard. Vi står inför många stora problem, till exempel klimatförändringar, uttömning av fossila energikällor (t. ex. petroleum, kol och naturgas) och miljöföroreningar. Därför är det brådskande att söka efter förnyelsebar energi och hur människor kan använda energi så effektivt och ändamålsenligt som möjligt. Högeffektiva material är viktiga för att utvinna och använda energi ändamålsenligt. Under de senaste åren har blyhalogenidperovskitmaterial blivit en typ av lovande och mångsidiga material avsedda för förnyelsebar energiproduktion, till exempel solceller. Blyhalogenidperovskitmaterial kan användas för att tillverka effektivare energiomvandlingsprodukter för vardagsbruk, t.ex. ljussättning (t.ex. lysdioder, LED:er), bildskärmar (t.ex. teveapparater), fotodetektorer (t.ex. kameror) och lasrar. Det finns absorption och emission av fotoner i alla produkterna. Under fotonabsorption och -emission sker många fotofysiska processer.

Omfattande kunskaper om blyhalogenidperovskitmaterialens fotofysik kommer att spela en viktig roll för att förbättra både materialens och produkternas funktion. I den här avhandlingen utforskade vi fotofysiken i perovskitkristaller av nanostorlek (1 nm = 0,000 000 001 m) och mikrostorlek (1 µm = 0,000 001 m) som kanske kan användas för LED:er, TV-apparater och fotodetektorer. Vi utforskade blyhalogenidperovskitnanokristallers stabilitet under ljusbestrålning.

Blyhalogenidperovskitnanokristaller kan bli ett aktivt medium för lasrar med tvåfotonabsorption (där två fotoner absorberas samtidigt). Därför utforskade vi tvåfotonabsorptionsprocessen i blyhalogenidperovskitnanokristaller. Sedan tillverkade vi en högeffektiv fotodetektor baserad på blyhalogenidperovskitmikrokristallager.

Det finns stora miljöproblem med att använda blyhalogenidperovskitmaterial som innehåller giftigt bly. Därför ersatte vi det giftiga blyet med mindre giftig vismut i perovskitnanokristaller. De vismutbaserade kristallerna fotoluminescerar med synligt ljus. Emissionsintensiteten är dock väldigt svag på grund av att laddningsbärare fastnar i fälltillstånd. Det är möjligt att begränsa fällorna och öka emissionsintensiteten för användning i LED:er.

Acknowledgement

4 years PhD study in Sweden has been a wonderful trip in my life. During this journey I have gained many precious things both in scientific research and daily life. “Darkness is always there. One just has to fight.” And this made me to become a happier and stronger person. I wish to thank the people who gave me the chance to develop and discover the non-scientific side of life. Furthermore, I would like to thank to the people who have helped and encouraged me to overcome the darkness. Without these people, I would not be able to finish this thesis. Below I would like to express my sincere gratitude to the people who have made my PhD study an enjoyable and fruitful experience.

Tonu, my main-supervisor, your openness and optimism encouraged me to continue my PhD study. I really appreciate the freedom that you gave me. Especially, the fact is that you made it possible for me to change my PhD research project twice in the 4 years. Your guidance helped me all the time during the research and writing of this thesis.

Atsunori, we are both from Asia with similar cultural backgrounds. You have made my life in Sweden much easier and more interesting. I will always remember what you have taught me: that a human should explore and be creative in both research and daily life instead of being a robot.

Karel, you have given me a lot of positive energy for my PhD study. I really enjoyed all the discussions with you.

Kaibo, you are always ready to discuss with me and trying your best to help me with my research. This helped my PhD thesis works to go smoothly.

All the Co-authors, thank you all for the work we did together. Especially, Pavel, thank you for teaching me how to use the transient absorption set-up, I would not be able to write this thesis without using the set-up. Bin, thank you for your visits - it was so much fun to do the projects together. Maria, I would like to thank you for spending time with me to help me with TEM for the NCs.

My Officemates, it was a lot of fun to discuss with you about both science and life. I learned a lot from all of you. Especially, Alex1, your presence in the office made the office so lovely. I really hope you have stayed here longer. Alex2, your jokes

are really creative and made my office time colourful. Marina, I really wish you would have joined us in our office earlier. You are such helpful and kind person.

Chemical Physics, Thanks to all the people from this department. You made this department to be a great place to do research. I really enjoyed the seminars, social activities, collaborations with other parts of the Chemistry Center and NanoLund. I would like to give special thanks to our administration staff, Maria, Thomas, Anki, Katarina, Annelie and Caroline for your help.

Komvux, Thanks to the whole group in the SFI class. Lärare Birgitta, Kursen kramar Anna, Jadranka, Hassan, Ahmad, Shirin, Ahmad, Irina... Tack så mycket för er kamratskap.

Thanks to Nils, Qi, Marina and Rui for proofreading the thesis.

Thanks to my parents and my sister who were always supporting me during my study and life.

Marek, Thank you so much for all the support. Especially, for bringing me to Chemistry Center everyday while I had fractured knee.

Thanks to all the people who were directly/in-directly helping with my PhD studying.

List of Publications

This thesis is based on the following papers, which will be referred to in the text by Roman numerals.

I. **Junsheng Chen**; Dongzhou Liu; Mohammed J. Al-Marri; Lauri Nuuttila; Heli Lehtivuori; Kaibo Zheng, "Photo-stability of $CsPbBr_3$ Perovskite Quantum Dots for Optoelectronic Application". *Sci. China Mater.*, 2016, 59, 719-727.

II. **Junsheng Chen**, Karel Žídek, Pavel Chábera, Dongzhou Liu, Pengfei Cheng, Lauri Nuuttila, Mohammed J. Al-Marri, Heli Lehtivuori, Maria E. Messing, Keli Han, Kaibo Zheng, Tõnu Pullerits, "Size Dependent Two-Photon Absorption Cross-Section of $CsPbBr_3$ Perovskite Quantum Dots". *J. Phys. Chem. Lett.*, 2017, 8, 2316–2321.

III. **Junsheng Chen**, Pavel Cháb̨era, Torbjörn Pascher, Maria E. Messing, Richard Schaller, Sophie Canton, Kaibo Zheng, and Tõnu Pullerits, "Enhanced Size Selection in Two-Photon Excitation for $CsPbBr_3$ Perovskite Nanocrystals". *J. Phys. Chem. Lett.*, 2017, 8, 5119–5124.

IV. Bin Yang, Fengying Zhang, **Junsheng Chen**, Songqiu Yang, Xusheng Xia, Tõnu Pullerits, Weiqiao Deng and Keli Han, "Ultra-Sensitive and Fast All-Inorganic Perovskite based Photodetector via Fast Carrier Diffusion", *Adv. Mater.*, 2017, 29, 1703758.

V. Bin Yang, **Junsheng Chen**, Feng Hong, Xin Mao, Kaibo Zheng, Songqiu Yang, Yajuan Li, Tõnu Pullerits, Weiqiao Deng, Keli Han, "Lead-Free, All-Inorganic Cesium Bismuth Halide Perovskite Nanocrystals with Long-Term Stability", *Angew. Chem. Int. Ed. Engl.*, 2017, 56, 12471–12475.

My Contribution to the Publications

I. I designed the experiments, synthesized the nanocrystals, performed the spectroscopy experiments together with Dongzhou, analyzed the experiment data, and drafted the manuscript.

II. I designed the experiments, synthesized the nanocryatals, performed the spectroscopy experiments, analyzed the experiment data, and drafted the manuscript.

III. I designed the experiments, synthesized the nanocrystals, performed the spectroscopy experiments, analyzed the experiment data, and drafted the manuscript.

IV. I designed the experiments together with Bin. I performed the time-resolved experiment part, analyzed the experiment data, and drafted the manuscript together with Bin.

V. I designed and performed the time-resolved experiment part, analyzed the experiment data, and drafted the manuscript together with Bin.

Other Publications are not included in the thesis

I contributed to these papers which are outside the scope of this thesis.

VI. **Junsheng Chen**, Bin Yang, Chuanshuai Li, Kaibo Zheng, Karel Žídek, and Tõnu Pullerits, ”Photostability of the Oleic Acid-Encapsulated Water-Soluble $Cd_xSe_yZn_{1-x}S_{1-y}$ Gradient Core–Shell Quantum Dots” *ACS Omega*, 2017, 2, 1922–1929.

VII. **Junsheng Chen**; Karel Žídek; Mohamed Abdellah; Mohammed J. Al-Marri; Kaibo Zheng; Tõnu Pullerits, "Surface Plasmon Inhibited Photo-Luminescence Activation in CdSe/ZnS Core-Shell Quantum Dots." *J. Phys.: Condens. Matter* 2016, 28, 254001.

VIII. Kaibo Zheng; Karel Žídek; Mohamed Abdellah; **JunSheng Chen**; Pavel Chabera; Wei Zhang; Mohammed J. Al-Marri; Tõnu Pullerits, “High Excitation Intensity Opens a New Trapping Channel in Organic–Inorganic Hybrid Perovskite Nanoparticles”. *ACS Energy Lett*., 2016, 1, 1154–1162.

Abbreviations

1PA	one-photon absorption
2D	2-dimensional
2PA	two-photon absorption
BBO	beta-barium borate
CB	conduction band
CIGS	copper indium gallium selenide
D^*	detectivity
DMSO	dimethyl sulfoxide
EBE	exciton binding energy
EQE	external quantum efficiency
EU	European Union
FA	formamidinium
FWHM	full width at half maximum
G	photoconductive gain
GSB	ground state bleach
IRF	instrument response function
LED	light emitting diode
LHP	lead halide perovskite
MA	methylammonium
MC	microcrystal
MEG	Multi-exciton generation
MOFs	metal-organic frameworks
NC	nanocrystal

NIR	near infrared
OA	oleic acid
OAm	oleylamine
ODE	1-octadecene
PL	photoluminescence
QD	quantum dot
QY	quantum yield
R	responsivity
RoHS	Restriction of Hazardous Substances
TA	transient absorption
TCSPC	time-correlated single photon counting
TEM	transmission electron microscopy
TRPL	time-resolved photoluminescence
UV-Vis	ultraviolet-visible
VB	valence band

Chapter 1: Introduction

1.1 Materials for Renewable and Sustainable Energy

Energy is the most valuable resource for industrialization. Since the first industrial revolution, people have achieved spectacular industrialization and development based on fossil fuels. The demand and consumption for energy is dramatically increasing due to the increased population, rising living standards and global industrialization. However, the consumption of fossil-fuel energy is problematic due to the limited stock and environmental issues it would cause including global warming and pollution. In order to fulfill the energy demand, it is important to seek for renewable and sustainable energy sources with low cost and high efficiency, and efficient ways of energy consumption.[1]

Material science is playing an important role in enabling technologies that can offer solutions to achieve progress towards renewable and sustainable energy production, storage and usage. With the advances in material science, we will be able to optimize the efficiency of power conversion from renewable energy sources, such as solar radiation and wind. New catalysts enable the fuel generation and chemical production directly from H_2O and CO_2 economically.[2] Global warming might also be solved by capturing and storing greenhouse gases such as CO_2, with novel materials, such as metal-organic frameworks (MOFs).[3] Moreover, new lighting technologies have emerged, for example, today the efficiency of white light LEDs is higher than conventional incandescent lamps by one order of magnitude.[4] The advantage of material science offers possibilities to utilize different forms of energy (such as solar, wind and thermal energy) and supply efficient energy consumption strategies.

Solar energy has long been considered as most promising renewable and sustainable energy source with the most abundance. Over the last decades, converting solar energy into electricity has been explored by using various photovoltaic materials such as silicon, organic dyes, conjugated polymers, quantum dots (QDs), perovskites, copper indium gallium selenide (CIGS), cadmium telluride (CdTe) and so on.[5] Over the past decades, solar-cell efficiency

has increased from ~1% to more than 40%,[6] which exhibits enormous potential of photovoltaics to meet the increasing global energy demand.

1.2 Perovskite Materials: Nanocrystals and Microcrystals, and Their Applications

In recent years, solar cells based on organic–inorganic hybrid LHP materials have shown a rapid growth of the power conversion efficiency from 3.8 % to more than 22% within less than 10 years.[7] Therefore, LHP materials have drawn significant attention from both fundamental and applied research.[8] The high performance of LHP-based solar-cells can be attributed to the exceptional optoelectronic properties, such as: a large absorption coefficient, a broad absorption band, a long charge-carrier lifetime and a high charge-carrier mobility. Moreover, their low cost solution processability facilitates the scale-up of the LHP solar-cell fabrication. Apart from solar cells, LHP materials also show application potential for other optoelectronic devices such as LEDs, photodetectors[9-10], and lasers[11-12].

Despite of promising application potential, the stability issues of LHP materials have not been fully resolved yet.[13] In particular, they tend to decompose induced by moisture, heat and light exposure. The instability is not only a hurdle to commercialization of such devices, but also makes it difficult to elucidate the photophysics in LHP materials. For instance, the photophysical properties are sensitive to a large range of factors, including preparation conditions, sample aging and ambient conditions during experiments. Nevertheless, a comprehensive understanding of the photophysics will be a key factor to further improve the performance of these devices.

1.2.1 The Crystal Structure of Perovskite

The mineral perovskite calcium titanium oxide ($CaTiO_3$), is the parent compound of the perovskite-structured family.[14] The chemical formula of perovskite materials is generalized as ABX_3, where A and B are two cations with different sizes, and X is an anion that binds to both A and B. The divalent metal cation, B^{2+}, has a 6-fold coordination and forms an octahedron unit together with the X^- anion. The octahedron units form a framework by sharing the corners (see Fig. 1.1). The monovalent cation A^+, fills the 12 coordinate cavities formed by the BX_3 network and is surrounded by 12 equidistant anions.[15] The idealized ABX_3 structure is a primitive cubic cell formed with A cations, face-centered X anions and a B cation occupying the center of the cube. However, the changing size or orientation of

cation A can result in a distortion to tetragonal or orthorhombic symmetries.[13, 16] Different symmetries bring different properties to the perovskite materials, and they induce for example different band gap energies in some materials, phase transitions at specific temperatures. These lattice-related properties are, however, out of the scope of this thesis. Figure 1.1 shows the structure of ABX_3 perovskites with cubic symmetry. The monovalent cation can be methylammonium (MA, $CH_3NH_3^+$), formamidinium (FA, $CH_2(NH_2)_2^+$), caesium (Cs^+), or rubidium (Rb^+); B stands for lead (Pb(II)) or tin (Sn(II)) and X for iodine (I^-), bromine (Br^-) or chlorine (Cl^-).[17]

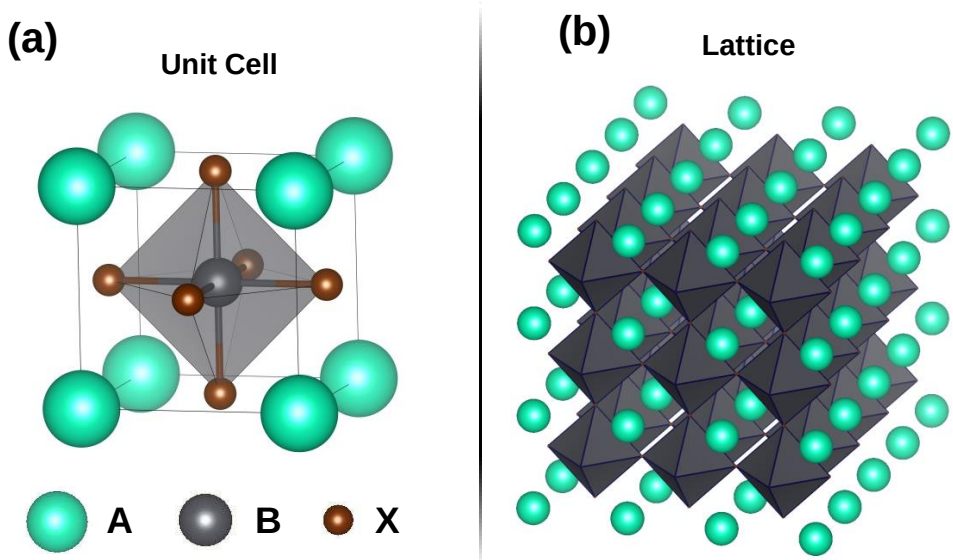

Figure 1.1
(a) Crystal sturcture of ABX_3 perovskites.[18] Green = A (i.e. MA, FA or Cs), gray = B (i.e. Pb or Sn) and brown = X(i.e. Cl, Br, or I). (b) 3-dimensinal perovskite lattice structure.[19]

1.2.2 Perovskite Nanocrystals

A large number of research and technology developments focus on photovoltaic devices based on LHP thin films. Such devices are close to the industrial standard.[20] Apart from their thin-film form, perovskite nanocrystals (NCs) have been recently reported, such as organic–inorganic ($CH_3NH_3PbBr_3$, $MAPbBr_3$) NCs[21] and all-inorganic caesium lead halide ($CsPbX_3$, X=Cl, Br, Cl) NCs.[22] Owing to their broadband absorption, easily tunable optical band gap and superior PL quantum yield (QY ~100%)[20], perovskite NCs are suitable materials for emitting devices such as displays, LEDs, and lasers.

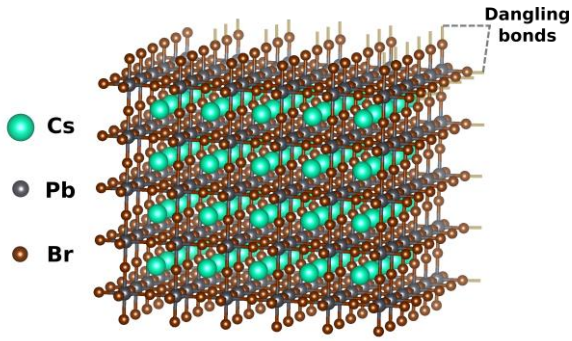

Figure 1.2
$CsPbBr_3$ NC without capping agent.

Colloidal NCs show enhanced PL emission compared to their bulk counterparts, due to efficient surface passivation and the increased exciton binding energy (EBE) in NCs.[23] In bulk semiconductor materials, unterminated bonds, also known as dangling bonds (Figure 1.2), are present both in bulk and on the surface. In NCs, such dangling bonds mostly occur on the surface. These unterminated dangling bonds can act as nonradiative traps, because they can capture the electrons/holes before they have a chance to recombine radiatively. Colloidal NCs offer the possibility to passivate the surface traps by introducing surface capping agent. The dangling bonds can be terminated by capping the NCs surface with organic molecular ligands. $CsPbBr_3$ NCs with capping agents (oleylammonium bromide and oleylammonium oleate) show a PLQY up to 90%.[22, 24] The PLQY of $CsPbBr_3$ NCs can be further improved to unity by passivating surface defects/traps with thiocyanate salt.[20] The increased EBE in NCs also plays an important role for the high PLQY in NCs. For example, the EBE of $MAPbBr_3$ NCs is more than 300 meV, about 4 times higher than the value of $MAPbBr_3$ bulk crystals (~80 meV).[23, 25] The significantly increased EBE can prevent the dissociation of the exciton prior to its radiative decay in NCs.[21] As a result, the PLQY can be increased from less than 0.1% (micrometer-sized $MAPbBr_3$ particles) to 70% ($MAPbBr_3$ NCs).[26] Moreover, the EBE of $CsPbBr_3$ materials can be engineered from ~30 meV to 120 meV by increasing the quantum confinement with size reduction.[27-31]

Quantum confinement cannot only alter the PL emission intensity of NCs by increasing the EBE but also change the optical absorption and PL emission spectra. As the NC size decreases, the quantum confinement is enhanced and both absorption and PL emission spectra will show a blue shift. The energy shift has been explained by using the particle-in-a-sphere model.[32] The size-dependent NC energy gap can be obtained from the following expression:

$$E_g = E_{bulk} + \frac{\hbar^2\pi^2}{2R^2}\left(\frac{1}{m_e} + \frac{1}{m_h}\right) - \frac{1.8e^2}{\varepsilon R} \qquad (1.1)$$

in which, E_{bulk} is the band gap of bulk material, $\hbar$ is Planck's constant, m_e and m_h are the effective mass of electron and hole, respectively, R is the sphere's radius; e is the elementary charge; and ε is the dielectric constant.

The second term of the right side of equation 1.1 is referred to as the confinement energy. The confinement energy increases with the decrease of the NC size as R^{-2}, and it can approach the bulk band gap energy E_{bulk} for small particles of narrow-band gap materials.[12] The third term of the right side is referred to as Coulomb e-h interaction, which increases with the decrease of NCs size as R^{-1}, and determines the EBE. In small size NCs, the confinement energy is usually much larger than the EBE.

A defect-tolerant electronic structure is another important reason for the high PLQY of LHP NCs. As shown in Figure 1.3a, in LHPs the band gap is formed between two sets of antibonding orbitals.[31] It has been reported that the band edge states are introduced by lead and halide.[33-35] The dangling bonds/vacancies form states which are located within valence band (VB) or conduction band (CB), or at worst, these states are 'shallow' defects close to the band edges,[31, 33, 36] which will not reduce the PL emission by acting as non-radiative decay centers. On the other hand, for conventional semiconductors (Figure 1.3b), the conduction band and valence band edge states are formed by anti-bonding and bonding orbitals, respectively. Hence, the nonbonding or weakly bonding orbitals reside deeply within the band gap and act as trap states.[31]

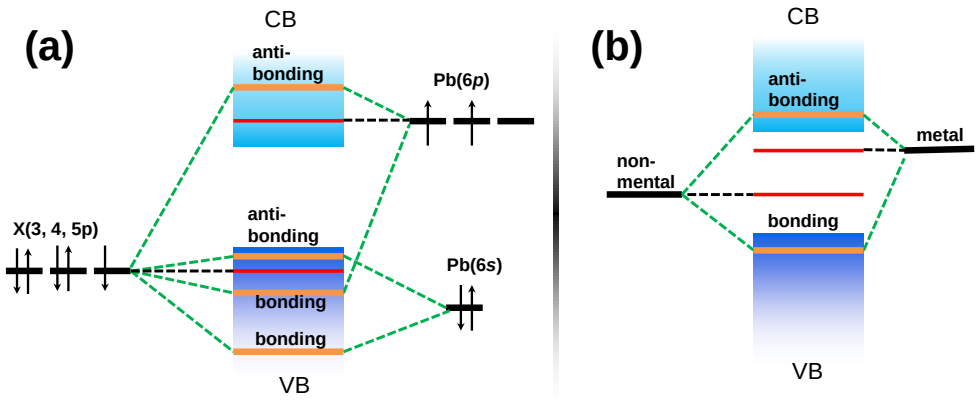

Figure 1.3
Comparing electronic structures that are defect-tolerant (a, for lead halid perovskites), and defect-intolerant (b, such as for conventional semiconductors, CdSe, GaAs, and InP). The red lines represent trap states formed by defects.

1.2.3 Perovskite Microcrystals

Numerous studies based on LHP thin films or centimeter/millimeter-sized single crystals have been carried out to fabricate solar-cells and photodetectors or to study the photophysics in the materials. However, none of these samples is suitable to study their intrinsic carrier recombination and transportation mechanisms. While thin films suffer from large differences between the grains and the grain boundaries, centimeter/millimeter-size single crystals are far larger than the carrier diffusion length (μm) and the photocarriers cannot be extracted efficiently. LHP micro-structures (or nanostructures) are ideal objects to study the carrier recombination and transportation processes, because they are free of grain boundaries and because of their suitable size. Furthermore, micrometer-sized perovskite crystals can be potentially applied for photodetectors with high responsivity, as their size is close to the charge carrier diffusion length.

1.3 Photophysics in Nanocrystals

A comprehensive understanding of the photophysics of NCs is important for their potential application in light emitting devices, photodetectors, lasers, solar-cells, sensing and photocatalysis. Various photophysical processes are involved in these NC-based devices, such as exciton generation, relaxation, charge carrier recombination and trapping.[37] It is possible to develop high performance devices based on understanding and utilizing these photophysical processes properly.

1.3.1 Excited-State Dynamics in Nanocrystals

A NC can be excited by a photon with energy higher than its band gap. Directly after the photoexcitation, the initial-generated electrons and holes occupy levels deep in the CB and VB with higher energy than the band edge as the excitation photon energy is higher than the band gap energy. Such electrons and holes with excess energy are referred to as "hot carriers", and they would undergo a rapid cooling process reaching the band edge. The excess energy is typically converted into heat on a picosecond timescale or even faster.[35, 37-41]

The excess energy can be utilized other than thermalization by different strategies (see Figure 1.4): (i) Hot-exciton emission, in which light emits from a hot-exciton state. This can be intraband hot-exciton emission (Figure 1.4a)[42] and interband hot-exciton emission (Figure 1.4b)[43]. Hot charge carriers can relax to the low energy level in the same band by emitting infrared photons. This is referred to as intraband hot-exciton emission. Interband hot-exciton emission means that two different hot charge carriers in different bands (an electron in the CB, a hole in the VB) recombine and emit a photon with energy higher than the band-gap energy, i.e. the emission spectra show a blue shift compared to the band-edge emission. The emission decays on a picosecond timescale or faster. (ii) Hot charge carrier injection via a fast charge transfer pathway (Figure 1.4c, on a few picosecond timescale) competes with the cooling process. Hot charge carrier injection offers a possibility to minimize the thermodynamic losses and enables solar cells with high light–electricity conversion efficiency.[44] (iii) Multi-exciton generation (MEG, Figure 1.4d), in which hot electron–hole pair with energy greater than twice the band gap energy can generate an extra exciton by using the excessive energy.[45-46] This process enables that two or more excitons are generated from one absorbed photon, thus high energy photons can be converted into usable energy more efficiently. It has been demonstrated that the quantum efficiency of NC-based solar cells can be more than unity by utilizing the MEG process.[47-51] In order to make all these processes efficient it is also important to reduce the cooling efficiency.

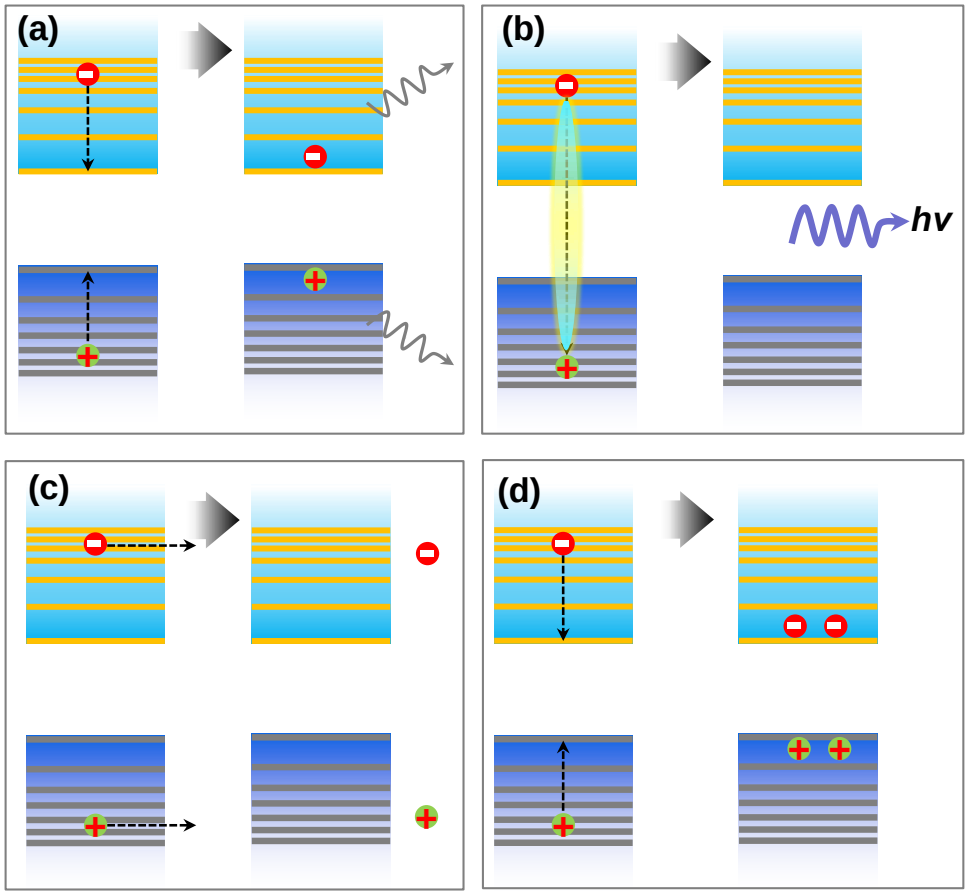

Figure 1.4
Relaxation pathways for hot-carrier states (a): intraband hot-exciton emission, (b) interband hot-exciton emission; (c): hot charge carrier injection, (d) Multi-exciton generation.

Auger decay plays an important role, when an electron–hole pair (an exciton) and one or more extra charge carriers are present in one NC (see Figure 1.5). In NCs, the Auger decay involves an electron-hole pair that recombines non-radiatively and transfers the energy to the other charge carrier that is excited to a higher excited state. Typically, Auger recombination involves trion or biexciton states. In the application of LED, bio-sensing and lasers, such Auger recombination is not desirable while would induce a loss of emission yield in these devices. To minimize the Auger recombination, NC charging and biexciton states should be avoided. This can be done by keeping the excitation intensity sufficiently low. However, for lasers, the excitation intensity must be high enough to reach the lasing threshold.

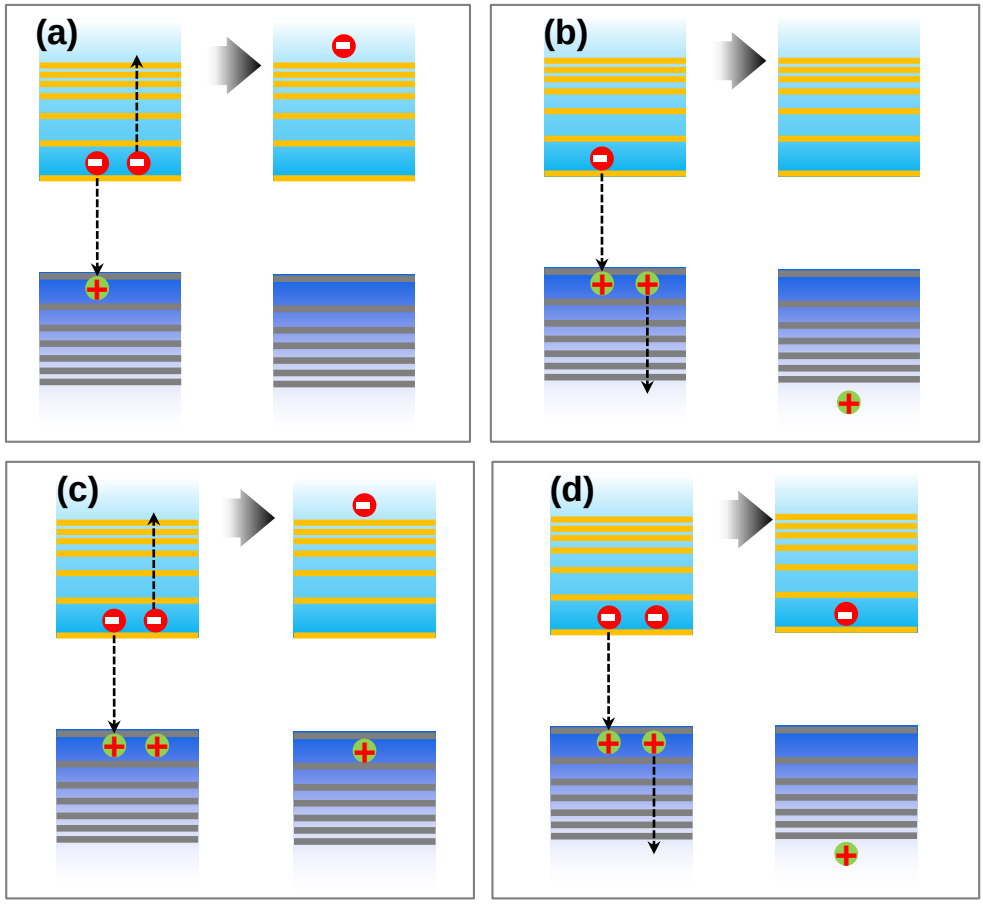

Figure 1.5
Auger decay pathways. (a): in the negative trion state, (b): in the positive trion state, (c, d): in the biexciton state.

Spontaneous radiative recombination is the desired exciton recombination pathway for NC applications in light emitting devices. After hot-exciton relaxation and Auger decay processes, the exciton reaches the band edge and recombines radiatively by emitting a photon (see Figure 1.6). The emitted photon energy and PL lifetime can be tailored by changing the composition, shape or size of the NCs. This can be easily achieved by modifying the growth time, capping agents or chemicals for preparation of colloid NCs. Beside band-edge radiative recombination, trapped charge carriers can also recombine radiatively emitting a lower-energy photon compared to band-edge recombination. This so-called trap PL (trap emission) is usually characterized by a low PLQY. Most of the trapped charge carriers recombine non-radiatively. Hence, trap/defect sites in NCs have to be minimized for light-emitting device applications.

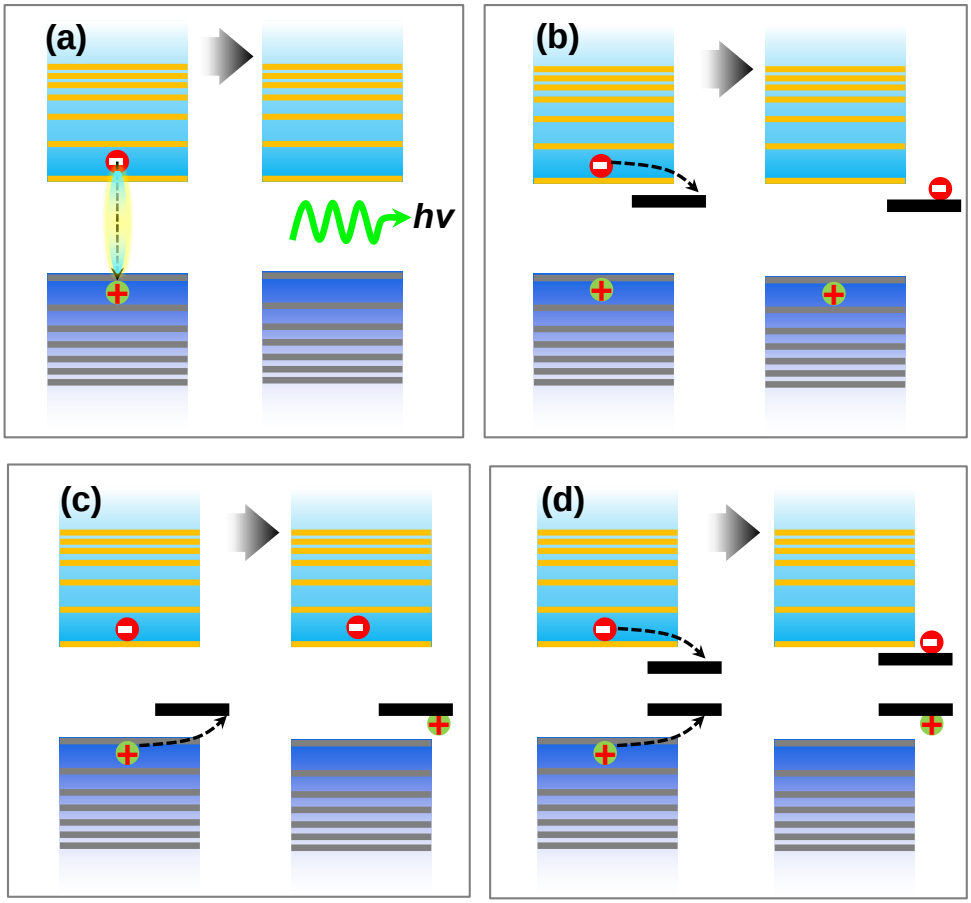

Figure 1.6
(a) Radiative recombination, (b): electron trapping, (c): hole trapping, (d): electron and hole trapping.

1.3.2 Two-Photon Absorption

Electron-hole pairs can be generated by absorbing photons with energy higher than or equal to the NC energy gap (eq. 1.1). However, NCs can absorb two photons of energy lower than the energy gap simultaneously, and generate an electron-hole pair. This process is called two-photon absorption (2PA), which was proposed by Göppert-Mayer in 1931.[52] Kaiser and Garrett reported experimentally 2PA-generated fluorescence in CaF_2:Eu^{2+} crystals in 1961.[53] In the 2PA process, two photons are absorbed simultaneously, and the 2PA probability increases with the square of excitation light intensity. Hence, 2PA can be observed with intense laser beam excitation, particularly with focused pulsed (fs~ps) lasers, which can generate high instantaneous photon intensities (>10^{14} photons/cm^2/pulse). The

quadratic intensity dependence enables three-dimensional localization of the excitation at a tight focal point. On the other hand, 2PA shows a longer penetration depth compared to one-photon absorption (1PA) for the same materials, because the 2PA excitation photon energy is usually in the NIR range. Compared to visible light, NIR light has a much longer penetration depth, because of the decreased absorption (NIR energy < bang gap) and reduced scattering of NIR light. Consequently, 2PA materials are currently attracting considerable attention in applications of bio-imaging,[54] bio-sensing, data storage,[55] frequency up-conversion lasing and amplification,[56] optical power limiting,[57] photodynamic therapy,[58] three-dimensional material micro-fabrication[55] and information technology.

Chapter 2: Experimental Methods

2.1 Synthesis of Perovskite Nanocrystals and Microcrystals

The solution-process-ability of LHP materials makes them attractive for low-cost mass-production. Such solution processing allows perovskite thin film solar-cells to hold a distinguished advantage over traditional silicon solar-cells from the simplicity point of view. Dense layers of well crystallized perovskite thin films can be obtained by spin-coating a lead halide and a methylammonium halide solution on a substrate.[59-60] Similarly to LHP thin films, the LHP NCs and MCs can be prepared by using the solution processing methods as well. In this thesis, the preparation methods of perovskite NCs and MCs will be discussed. Thin film LHP materials are out of the scope of this thesis.

2.1.1 Synthesis of Perovskite Nanocrystals

Two different approaches were used to prepare perovskite NCs. One is the traditional hot-injection method which was widely used for synthesis of CdSe NCs[61]. Another method is the anti-solvent precipitation crystallization,[26] which was utilized to synthesize other NCs.[26, 62-63] Specifically, $CsPbBr_3$ LHP NCs were prepared by using the hot-injection method and lead-free $Cs_3Bi_2Br_9$ NCs were prepared by using the anti-solvent precipitation method.

2.1.1.1 Synthesis of $CsPbBr_3$ Lead Halide Perovskite Nanocrystals

$CsPbBr_3$ colloidal NCs were prepared by using a method developed by Protesescu et al.[22] 0.814 g Cs_2CO_3 (Sigma-Aldrich, 99%) were mixed with 40 mL 1-octadecene (ODE, Sigma-Aldrich, 90%) and 2.5 mL oleic acid (OA, Sigma-Aldrich, 90%), kept at 120 ℃ and degassed for 1 hour. The mixture was heated up to 150 ℃ for 30 min under N_2 atmosphere. Obtained Cs-oleate was kept in a glove box and heated up to 100 ℃ before using. Next, 0.689 g $PbBr_2$ (Sigma-Aldrich, 99.999%) and 10 mL ODE were degassed for 1 hour at 120 ℃, afterwards 0.5 mL dry oleylamine (OAm, Sigma-Aldrich, 80−90%) and 0.5 mL OA were added and heated up to 120 ℃ under N_2 atmosphere. To control the NC size, the temperature

was increased to different levels between 140 ℃ and 200 ℃, then 0.4 mL Cs-oleate solution were rapidly injected. After injection, the mixture solution was immediately cooled by an ice-water bath. The injection temperature was set to 140 ℃, 150 ℃, 160 ℃, 180 ℃ and 200 ℃ to obtain particles with mean size of 4.6, 5.2, 6.9, 9.4 and 11.4 nm, respectively.

We used two different methods to isolate NCs with various sizes. For larger size NCs synthesized at 160–200 ℃, the ice-water cooled crude solution was centrifuged at 6500 RPM for 10 min. After the centrifugation, the supernatant was discarded and the particles were re-dispersed in toluene. In order to obtain narrow size distribution of NCs, the solution was centrifuged at 2500 RPM for 5 min again. After this centrifugation, the supernatant was collected. For smaller size NCs synthesized at 140 and 150 ℃, the crude solution was centrifuged at 6500 RPM for 15 min. After the centrifugation, the supernatant was collected as solution A, and then 2-propanol (Sigma-Aldrich, 99.5%) was added into the solution A ($V_{2\text{-propanol}}$:$V_{\text{solution A}}$ = 3:1). 2-propanol can be helpful for precipitation of NCs. The mixture of solution A and 2-propanol was centrifuged for 10 min at 6500 RPM. After centrifugation, the supernatant was discarded and the particles were redispersed in toluene.

2.1.1.2 Synthesis of $Cs_3Bi_2Br_9$ Nanocrystals

For ligand-free $Cs_3Bi_2Br_9$ NCs, CsBr (Sigma-Aldrich, 99.999%) and $BiBr_3$ (Sigma-Aldrich, ⩾98%) with molar ratio 3:2 were dissolved in dimethyl sulfoxide (DMSO, Sigma-Aldrich, ⩾99.5%) to form a precursor solution. For example, 90 μmol CsBr (19.2 mg) and 60 μmol $BiBr_3$ (26.9 mg) were dissolved in 2 mL DMSO to form a 15 μM $Cs_3Bi_2Br_9$ precursor solution. 200 μL precursor solution was injected into 5 mL 2-propanol, under vigorous stirring for about one minute. Then, the solution was centrifuged at 6000 RPM for 5 min to discard the large particles. After that, clear yellow-green colloidal NCs were obtained. A similar approach was used to prepare ligand-free $Cs_3Bi_2X_9$ (X=Cl, Br, I) NCs.

For OA-capped NCs, 0.3-0.5 mL OA were added in 5 mL 2-propanol. Then 200 μL CsBr and $BiBr_3$ precursor (as mentioned above) were injected into the 5 mL 2-propanol with OA added under vigorous stirring. After that, the solution was centrifuged at 6000 RPM for 5 min. The supernatant with NCs was collected. A similar approach was used to prepare OA-capped $Cs_3Bi_2X_9$ (X=Cl, Br, I) NCs.

2.1.1.3 Nanocrystal Characterization

UV-Vis absorption spectra were obtained using a PerkinElmer Lambda 1050 spectrophotometer. Steady-state fluorescence spectra were recorded using a Horiba Jobin Yvon Fluorolog-3 spectrofluorometer. The size of the NCs was characterized by high-resolution analytical transmission electron microscopy (TEM, Jeol 3000F). The sizes of $CsPbBr_3$ NCs were measured along their edges.

Due to deviation from cubic shapes, the lengths of the long edge and the short edge were measured for each NC.

2.1.2 Synthesis of Lead Halide Perovskite Microcrystals

Different methods were developed for organic–inorganic LHP single crystal growth. They can be divided into four categories: solution temperature-lowering method, inverse temperature crystallization method, anti-solvent vapor-assisted crystallization method and melt crystallization method.[64-66] In this thesis, perovskite MCs were synthesized by a modified solution inverse temperature crystallization method.[67]

2.1.2.1 Synthesis of $CsPbBr_3$ Lead Halide Perovskite Microcrystals

$CsPbBr_3$ MCs were prepared by using a method developed by Saidaminov et al.[68] CsBr (3 mmol) and $PbBr_2$ (6 mmol) were dissolved in 3 mL DMSO. The solution was sonicated for 1 hour until all the chemicals were dissolved. Then it was gradually heated up to 100 ℃ in a silicone oil bath. The appearing yellow and orange crystals ($CsPb_2Br_5$ crystals) were filtered out by a syringe filter (pore size of 200 nm). In order to obtain an interconnected $CsPbBr_3$ MC layer, the filtrate was diluted 3 times at room temperature. Toluene (as anti-solvent) was added dropwise under stirring until it reached saturation. The diluted solution (with toluene added) was heated up to 120 ℃. It was stirred to generate a high and homogeneous density of nuclei for crystallization.[69]. A glass substrate was added to the solvent for 3 mins, so that a thin layer of $CsPbBr_3$ MCs were formed on it. The substrate with the MC layer was heated up to 140 ℃ for 10 min under ambient atmosphere to evaporate the remaining solvent and highly crystalline $CsPbBr_3$ MCs were obtained.

2.2 Time-Resolved Photoluminescence Spectroscopy

The perovskite NCs and MCs, which we were studying, emit PL. This enables us to study the excited-state dynamics in these materials by time-resolved photoluminescence (TRPL) spectroscopic method. Two different TRPL spectroscopic methods were used here: time-correlated single photon counting (TCSPC) and a streak camera. The two techniques have a similar working scheme, as shown in Figure 2.1. A pulsed laser beam is focused on the sample. The PL from the sample is collimated and collected by a photodetector.

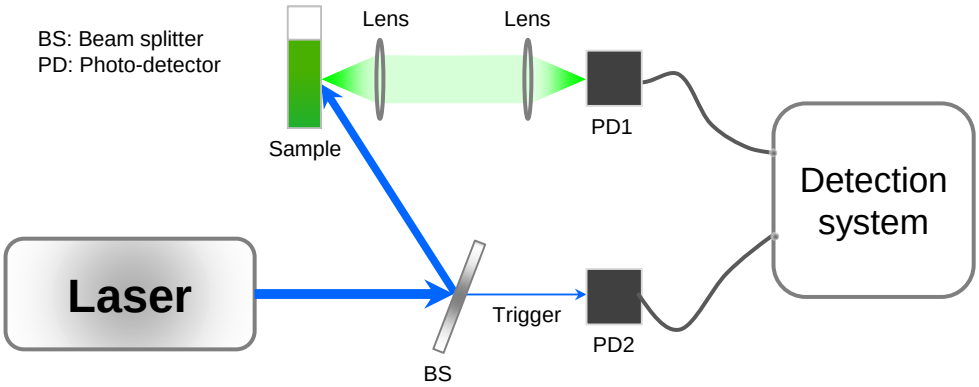

Figure 2.1
Time-resolved photoluminescence spectroscopy set-up scheme.

2.2.1 Time-Correlated Single Photon Counting

TCSPC is a statistical method for measuring PL lifetime with high sensitivity (single-photon level).[70] The principle of TCSPC is shown in Figure 2.2. The high sensitivity of TCSPC is based on the fact that only one emitting photon per exciting laser pulse is detected. The laser driver controls the laser head to generate a laser pulse and gives a start signal to the detection system as well. After a certain time delay of each laser pulse (start signal), once the detection system detects the first emitted photon from the sample, it stops to detect the rest of the emitting photons from the same excitation pulse. The collection method makes sure that no more than one photon per pulse is detected by the system. The event is stored in different channels corresponding to certain delay time ranges. This process is repeated over a large number of cycles, building up a histogram of detected photons in different channels. The delay time information is obtained by converting time to a voltage ramp.

The time resolution of a TCSPC set-up can be characterized by its *instrument response function* (IRF). Typically, the time resolution is limited by the detection speed of photodetector. The time uncertainty of different detectors can range from 25 ps to 400 ps.[71] Moreover, the IRF can be broadened by other factors, such as the excitation source and the timing jitter of the electronic components. In our work, a pulsed diode laser, triggered externally at 2.5 MHz, was used to excite the sample at 438 nm. The pulse duration of the laser was about 200 ps. The scattered laser light was blocked by a 450 nm long pass filter and the emitted photons were focused onto a fast avalanche photodiode (SPAD, Micro Photon Devices) with response time less than 50 ps. The full width at half maximum (FWHM) of the IRF is about 350 ps.

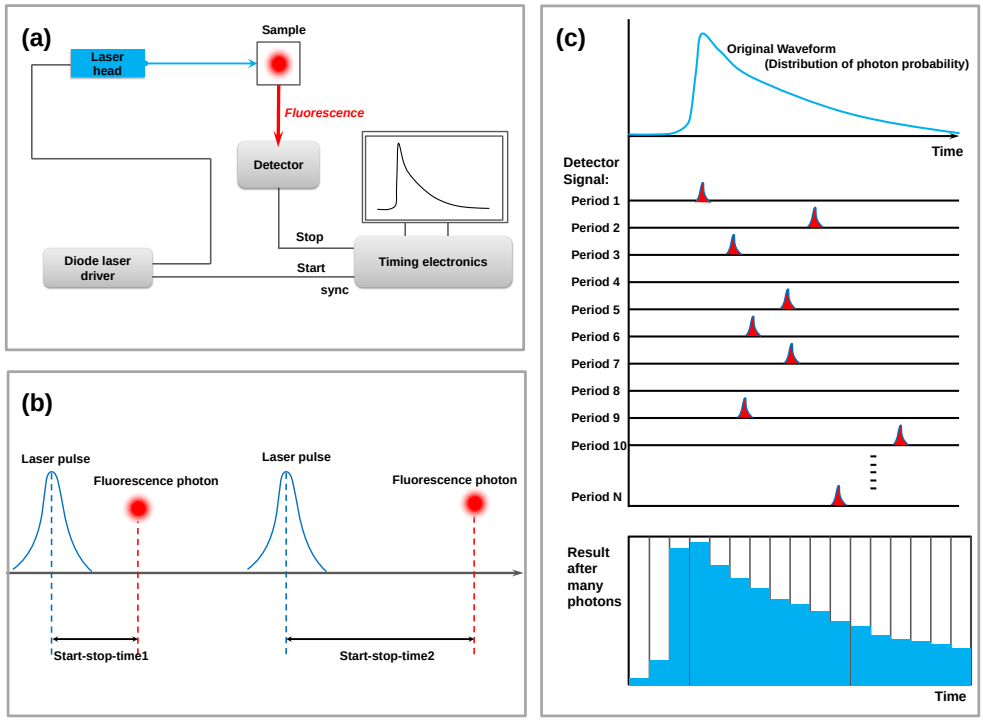

Figure 2.2
The principle of TCSPC: (a) experimental set-up for fluorescence decay measurements with TCSPC; (b) Measurement of start-stop times in time-resolved fluorescence measurement with TCSPC; (c) TCSPC measurement principle.

2.2.2 The Streak Camera

The streak camera can obtain simultaneously intensity, temporal and spectral information about the PL. In principle such 2-dimensional (2D) images can be acquired from only one excitation pulse. The principle of the streak camera is presented in Figure 2.3. Photons are emitted from the sample after excitation from a laser pulse. The PL is collimated and focused into a spectrograph. The photon energy is resolved by the spectrograph in space. Photons with different energy hit the photo-cathode, where they are converted into electrons. The photo-generated electrons are accelerated by an accelerating mesh, which gives a certain velocity to the electrons. The electrons go through a sweep electrode and the sweep circuit is triggered by a triggering signal, which is synchronized with the laser pulse. Hence, the delay time between the emitted photons and the excitation pulse can be obtained from the vertical deflection of the photo-generated electrons at a phosphor screen. Before reaching the phosphor screen, the photoelectrons are amplified by a micro-channel plate. The photoelectrons are converted into photons

by the phosphor screen and a 2D image with intensity, temporal and spectral information is recorded by a CCD camera.

In this work, the laser pulses were generated from a Ti:sapphire passively mode-locked femtosecond laser (Spectra-Physics, Tsunami), at 800 nm with 2 kHz or 80 MHz repetition rate and 150 fs pulse length. For 800 nm excitation, the laser pulses were used directly. For 400 nm excitation, the 400 nm pulses were generated by frequency doubling in a beta-barium borate (BBO) crystal.

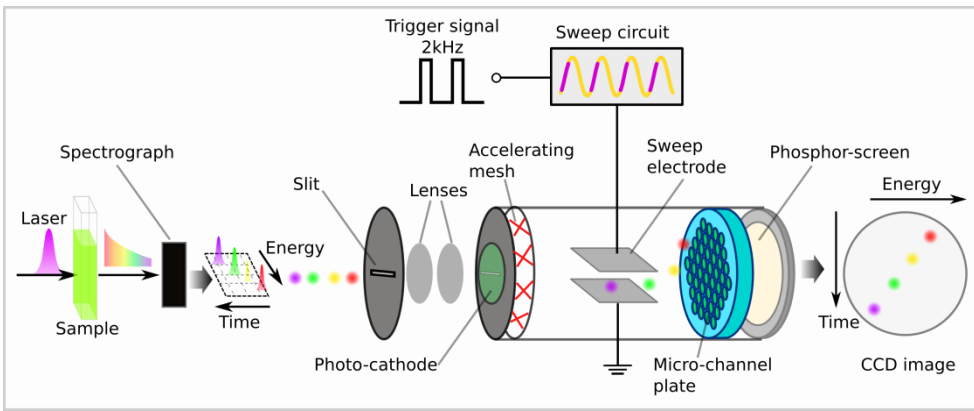

Figure 2.3
Streak camera principle.

2.2.3 Transient Absorption

Femtosecond transient absorption spectroscopy (TA) is an extension of steady-state absorption spectroscopy with ultrafast (sub-ps) time resolution. In steady-state spectroscopy, the absorption of the NCs is observed when they are in the ground sate. In TA, firstly the NCs are excited by one laser pulse (the pump beam), then the absorbance of another laser pulse (the probe beam) is detected by the detection system. The TA spectrum can be obtained by subtracting the absorbance of the probe beam with and without the pump beam which can be done by blocking the pump with a chopper. A transient absorption spectrum with time and energy resolution can be obtained by repeating this at different delay times between the pump and the probe pulse.

In this work, the TA experiments were carried out with a femtosecond pump–probe setup. The scheme of the setup is shown in Figure 2.4. A femtosecond oscillator (Tsunami, Spectra Physics) was used to seed a regenerative amplifier (Spitfire XP Pro), which provides intense femtosecond laser pulses (800 nm, 1 kHz repetition rate, 120 fs pulse length, 3 mJ/pulse). The pump pulses at 400 nm

were generated by a BBO crystal as a second harmonic of the laser pulse. The pump pulses at 800 nm were obtained directly from the regenerative amplifier. The pump pulses at other wavelengths (such as 675 nm, 725 nm, 870 nm and 950 nm) were generated by an optical parametric amplifier (Topas, Light Conversion). For the probe, we used broad-band super-continuum white light or narrow-band laser pulses. We obtained the broad-band super-continuum white light from a thin CaF_2 plate (TA spectra measurements). The narrow-band probe pulses (wavelength tuned from 470 nm to 513 nm) were generated by Topas1. By placing a Berek compensator in the pump beam, the mutual polarization between pump and probe beams was set to the magic angle (54.7 °). During the experiments, the samples were flowed or being stirred constantly to avoid photo-damage.

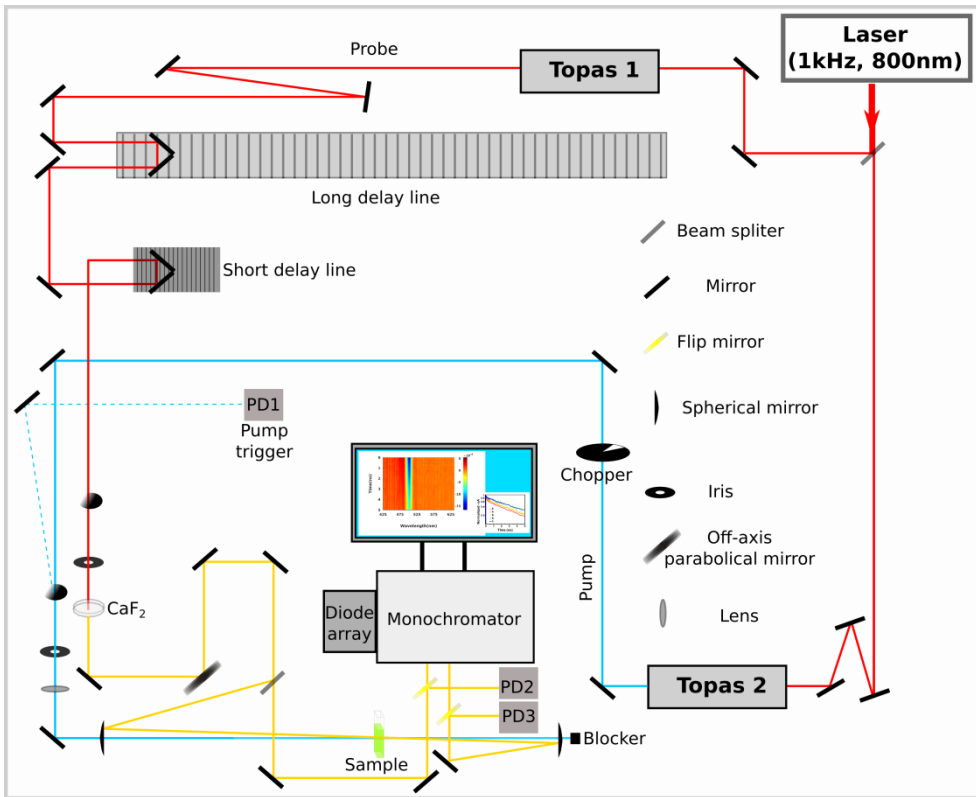

Figure 2.4
Transient absorption setup used in this work. The broad-band super-continuum probe pulses were detected by using a monochromator and diode array. The narrow-band probe pulses were detected by using two photodetectors (PD2 and PD3).

For the probe detections, we used two different detection systems (see Figure 2.4). The broad-band super-continuum probe pulses were detected by using a monochromator and diode array. The narrow-band probe pulses were detected by using two photodetectors (PD2 and PD3). PD1 is used as a pump trigger in both detection systems. Two delay lines are used in the setup: the long delay line with up to 9 ns delay time can be used for system with long excited-state lifetime; the short delay line with 10 fs time accuracy can be used for system with short excited-state lifetime.

2.3 Two-Photon Absorption Cross Section Measurement

The 2PA cross section ($\sigma^{(2)}$) is one of the most important characteristic parameters for 2PA materials (such as 2PA fluorophores, NCs). However, the value of $\sigma^{(2)}$ can be strongly influenced by the measurement methods. The most widely used methods to measure $\sigma^{(2)}$ are Z-scan and two-photon excited fluorescence. The Z-scan method detects the absorption directly at the excitation energy. Therefore, this method could be easily affected by the thermo-optical effect, strong background[72-73] and nonlinear scattering[74], which can give misleading 2PA cross-section results based on the Z-scan method. The two-photon excited fluorescence method requires the 2PA materials to exhibit PL which can be a limit for non-emissive materials. Furthermore, this method assumes that the materials have the same PLQY under two- and one-photon excitations. However, this does not always have to be true, due to the fact that 1PA and 2PA have different selection rules, and as a result different excited sates can be reached by 1PA and 2PA.[75] The different excited sates might couple to different nonradiative states. This might induce different PLQY under two- and one-photon excitations.

In this work, we used TA spectroscopy to measure the 2PA cross section of $CsPbBr_3$ NCs. This approach measures the 2PA-induced ground state bleach (GSB) signal, which can avoid thermo-optical effects and is background-free. The experimental details are described in the paper II[76]. However, to give a brief description about the experiment, at the weak excitation-intensity limit (the average number of excitons per NCs has to be smaller than 1), the exciton density can be related to the excitation intensity and the 1PA and 2PA coefficients. Meanwhile, the GSB signal can be related to the excitation intensity as well. Consequently, the 2PA coefficient can be obtained from the known 1PA coefficient, and $\sigma^{(2)}$ can be calculated from the 2PA coefficient and the NC concentration.

The excitation fluence of the pump pulse is critical for determining the value of $\sigma^{(2)}$. The excitation fluence was measured based on the excitation power and the spot size. The excitation power was measured several times during the experiment

by power meters, and the average value was used for data analysis. A Si-based power meter (FieldMaxII-TO, Coherent) was used for measuring the power of the 400 nm pump beam, which has low power (0.1 μW~60 μW). A thermal effect-based power meter (Model 1918-C, Newport) was used for measuring the power of the 800 nm pump beam, which has a high power (0.5 mW~5.4 mW). The spot size was measured by using a profile sensor (S9132, Hamamatsu) made by Pascher Instruments AB. In order to improve the homogeneity and obtain a symmetrical intensity distribution of the pump beam, three pinholes were placed along the pump beam. The first pinhole was used to obtain diffraction pattern by changing the size of the pinhole. The second and third pinholes were used to select the Airy disk and control the size of the pump beam. The measured excitation fluence error is under 20% of the fluence value. To avoid inhomogeneity of the excitation within the probe spot, the pump beam was loosely focused by using a lens with focal length 1000 mm making the pump beam profile much bigger than the probe beam.

Chapter 3: Stability of $CsPbBr_3$ Nanocrystals

Colloidal NCs show wide application potential in different fields, where they act as photoactive material (both photoabsorption and emission). Hence, it is critical that NCs show high photostability for their applications in solar-cells, LEDs, lasers and so on. However, most NCs show instability under light irradiation. For example CdSe, CdS and PbS NCs show photoactivation, i.e. a PL enhancement after irradiation with light,[77-79] absorption spectrum shift,[80] or decreased absorbance.[81-82] $CuInS_2$ NCs show PL quenching under light irradiation.[83] These changes of PL and absorption in NCs can be related to photooxidation,[79] photoannealing, stabilisation with surfactant molecules or surface-ligand passivation. In general, these processes are due to changes on the NC surface. Therefore, capping ligands on the NC surface play an important role for NC colloidal stability and photostability of NCs.[84-86] In paper I, we studied the stability of $CsPbBr_3$ NCs.

3.1 Highly Dynamic Ligand Binding in $CsPbBr_3$ Nanocrystals

Oleylammonium bromide and oleylammonium oleate are acting ligands in $CsPbBr_3$ NCs.[24] As shown in Figure 3.1, the oleylammonium cation binds to bromine on the NC surface through electrostatic interactions or a hydrogen bridge.[24, 87] The bromine or oleate anion interacts with caesium or lead ions on the NC surface. A recent report suggests that oleylammonium ions are the active capping agent, but a critical ratio of oleic acid and oleylamine is necessary for stabilizing $CsPbBr_3$ NCs.[87] The ligands show ionic and highly dynamic character, and this enables molecules and[88] metal cations[89] to adsorb on the NC surface for studying interfacial electron and hole transfer,[88] or metal cation sensing[89] in organic solution. However, the highly ionic dynamic ligand binding might destabilize $CsPbBr_3$ NCs, especially under photon irradiation, when charge carriers are generated.

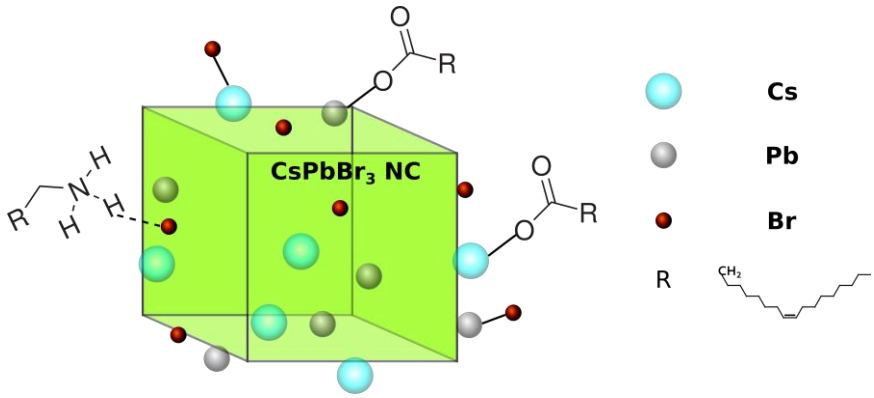

Figure 3.1
Scheme of $CsPbBr_3$ NCs surface ligands. The oleyammonium cation binds to surface bromine, bromine or oleate anion binds to caesium or lead cations on the NC surface.

3.2 Photostability of $CsPbBr_3$ Nanocrystals

The instability of perovskite materials towards moisture, light and heat has been the most significant barrier to widespread implementation of corresponding devices.[13, 90-91] The stability of $CsPbBr_3$ NCs under pulsed laser irradiation or heat has been tested.[92-93] However, more environmental conditions (such as temperature, light condition and atmosphere) need to be considered for working devices. In particular, the stability of colloid $CsPbBr_3$ NCs is a critical factor for the production and storage of $CsPbBr_3$ NCs inks for printed electronics and optoelectronics devices. In paper I, we studied the stability of $CsPbBr_3$ NCs in toluene under different conditions by using spectroscopic methods.

3.2.1 $CsPbBr_3$ Nanocrystals under Different Storage Conditions

The $CsPbBr_3$ NCs in toluene have been stored at different conditions for a stability study (see table 3.1). The samples were stored in seven different conditions: two different temperatures (room temperature and 4 ℃), two different atmospheres (air and N_2), and four different light irradiations (dark, LED irradiation and different filters applied) for studying temperature, atmosphere and light irradiation dependent stability.

Table 3.1.
Sample storage conditions

Sample	Temp.	Atmosphere	Light Condition[a]
S1	Room Temp.	N_2	Dark
S2	Room Temp.	Air	Dark
S3	4 ℃	Air	Dark
S4	Room Temp.	N_2	LED
S5	Room Temp.	Air	LED
S6	Room Temp.	Air	LED+filter1
S7	Room Temp.	Air	LED+filter2

[a] The LED lamp is from ORLED, model: RL18 (50 mW/cm^2), 440 lm, filter1 is a 300-500 nm band-pass filter, filter2 is a 550 nm long pass filter.

3.2.2 Instability of $CsPbBr_3$ Nanocrystals under Light Irradiation

The absorption and PL spectra of samples under light irradiation exhibit pronounced changes with time (see Figure 3.2) relative to the samples that were stored in the dark. The reduced absorbance indicates that the NC concentration is continuously decreasing. Moreover both the PL and the absorption edge show a red shift with time. These may be attributed to the weakening of the quantum confinement, that is to say the size of NCs is increasing and approaching the size of the exciton Bohr diameter in $CsPbBr_3$ (12 nm).[94] Together with the decreased PL intensity, a slow PL decay channel becomes dominant, as shown in Figure 3.2f. Furthermore, we can assign the slow decay channel to trap states involved PL decay. Compared with light irradiation, the atmosphere (air and N_2) and temperature (room temperature and 4 ℃) does not seem to play a big role for the long-term stability during storage, which has been discussed in paper I.

In order to understand the instability of $CsPbBr_3$ NCs from a microscopic point of view, we characterized the NCs of the samples S2 and S5 via TEM, as shown in Figure 3.3. The $CsPbBr_3$ NCs have a quasi-cubic morphology in sample S2. Due to the light irradiation, the $CsPbBr_3$ NCs trend to form (sinter) larger crystals. This morphology change agrees with the red-shifted absorption and PL spectra.

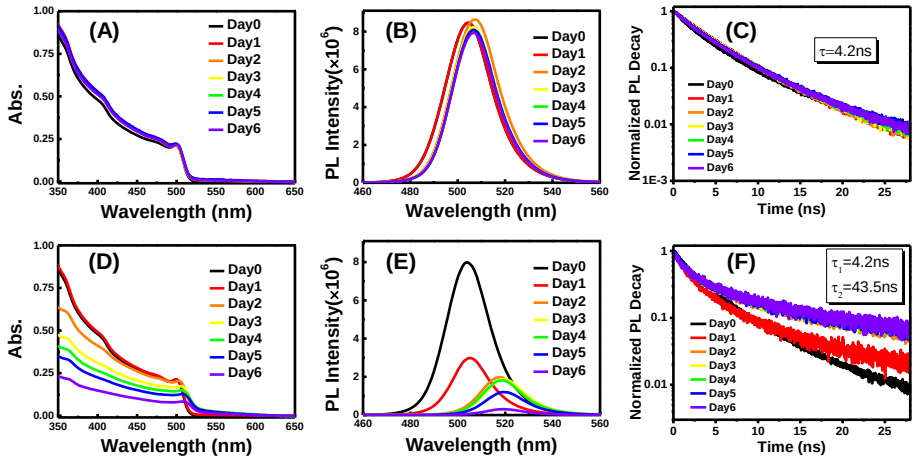

Figure 3.2
Absorption spectra, PL spectra and PL decay of samples S2 (upper panel a-c) and S5 (lower panel d-f) at different times.

The $CsPbBr_3$ NCs show instability under light irradiation. Based on the spectra and morphology changes, we propose the photoinduced degradation mechanism presented in Figure 3.3e. Due to the high carrier mobility[95] and fast interfacial charge transfer in $CsPbBr_3$,[88] photogenerated charge carriers can diffuse to the NC surface. Then the charge carriers are ready to be captured by ionic ligands on the NC surface. The highly ionic dynamic ligands can be removed from the surface more easily. As a consequence, uncapped NCs surfaces are formed leading to aggregation with neighboring particles.

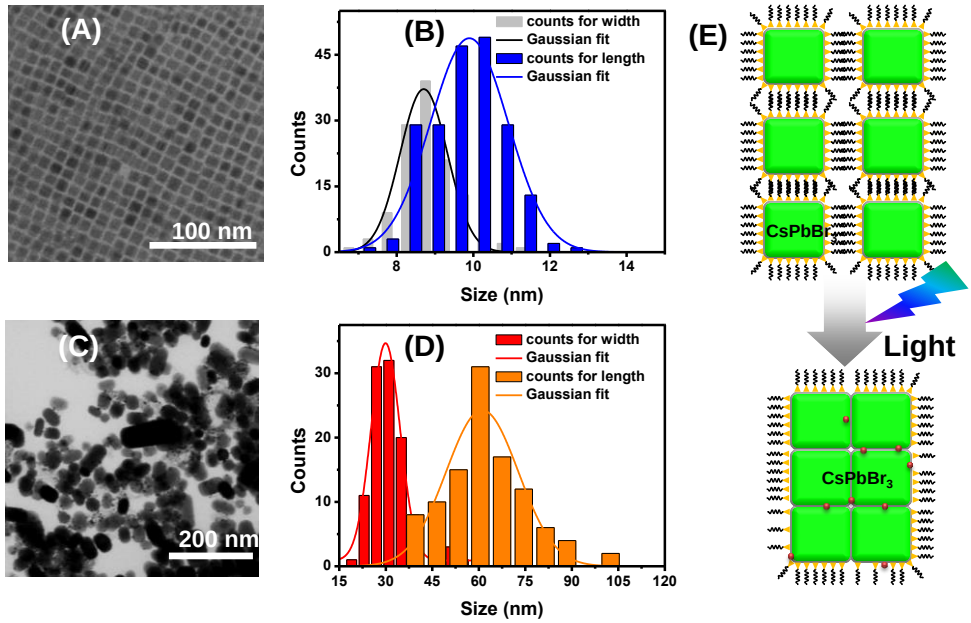

Figure 3.3
TEM images and size distribution histrograms measured along the long edge (length) and the short edge (width), (a) and (b) correspond to sample S2, (b) and (d) correspond to sample S5. (e) Schematic picture of the photodegradation of $CsPbBr_3$ NCs in toluene.

Chapter 4: Photophysics of Two-Photon Excited $CsPbBr_3$ Nanocrystals

A large 2PA cross section is one of the most desired properties for 2PA material applications. Compared to traditional organic 2PA molecules, semiconductor NCs show superior 2PA. Moreover, $CsPbBr_3$ NCs show orders of magnitude higher 2PA cross section compared to traditional NCs (eg. CdSe, CdTe). This increase is mainly related to the larger typical size of $CsPbBr_3$ NCs. Prototypes of two-photon-pumped lasers based on these NCs have been developed with outstanding performance.[96-97] However, the details of the photophysics under 2PA are yet to be investigated. In paper II and III, we studied the photophysics in $CsPbBr_3$ NC under 2PA.

4.1 Two-Photon Excited Photoluminescence of $CsPbBr_3$ Nanocrystals

$CsPbBr_3$ NCs show red-shifted PL emission and increased PL lifetime under 2PA compared with PL emission under 1PA, as shown in Figure 4.1. However, the different PL emission and decay have been ignored by previous reports.[96, 98-99] This is due to the red shift of PL emission that is just around 1-2 nm, as shown in Figure 4.1a. The PL decay is excitation intensity-dependent because of the Auger process that occurs once multiple excitons are generated. Moreover, there are different speculations about the reason for the different PL emission and decay, such as reabsorption, a different electronic relaxation process or size inhomogeneity.[96-97, 100]

The PL spectra were carried out with highly diluted samples (~15 nmol/L), and at this concentration the reabsorption effect is negligible. However, the 2PA-induced PL spectrum still shows a red shift compared to the 1PA-induced PL spectrum, as shown in Figure 4.1a. Hence, we can exclude reabsorption as the origin of such red-shifted PL emission.

The red-shifted PL spectra and different PL decay kinetics might be related to the selection rules for 2PA and 1PA processes leading to different initially excited states, or size inhomogeneity.

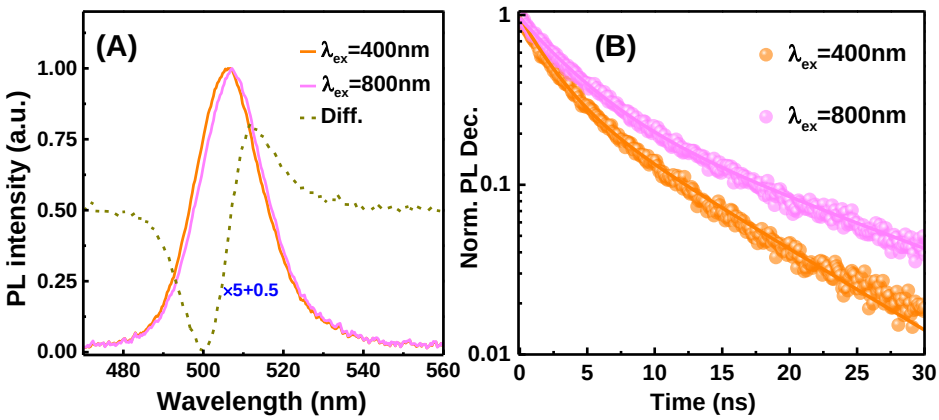

Figure 4.1
(a) One-photon excited PL spectrum (orange curve), two-photon excited PL spectrum (magenta curve) and the difference (Diff.) between two- and one-photon PL spectra (dark yellow dots curve) to highlight the difference between the two PL spectra from a solution of $CsPbBr_3$ NCs (~15 nmol/L). (b) PL decay trace of $CsPbBr_3$ NCs under low excitation fluence for one- and two-photon excitation (I_{400}=2.0×10^{11} photons/cm^2, I_{800}=1.0×10^{15} photons/cm^2, corresponding to *N*~0.02).

4.2 Two-Photon Absorption Process in $CsPbBr_3$ Nanocrystals

2PA is generally described in terms of a process which involves an initial state, an intermediate state and a final state, as shown in Figure 4.2. 2PA can be classified as degenerate and non-degenerate 2PA processes.[101] For degenerate 2PA, the two absorbed photons have the same energy (wavelength). For non-degenerate 2PA, the two absorbed photons have different energy. In this work, the used femtosecond laser pulse has up to 20 nm FWHM. To simplify, we treat the 2PA in $CsPbBr_3$ NCs as the degenerate case. The 2PA coefficient $\alpha^{(2)}$ can be defined as:

$$-\frac{dI}{dx} = \alpha^{(2)} I^2 \qquad (4.1)$$

in which, I is the excitation light intensity, x is the light propagating direction, and $\alpha^{(2)}$ can be represented as:

$$\alpha^{(2)} \propto \left| \sum_m \frac{\langle f | \vec{\mu}_{fm} \cdot \vec{E}_0 | m \rangle \langle m | \vec{\mu}_{mi} \cdot \vec{E}_0 | i \rangle}{E_{fi} - 2\hbar\omega} \right|^2 \qquad (4.2)$$

$|i\rangle$ is an initial state, $|m\rangle$is the manifold of intermediate states, $|f\rangle$ is a final state, E_{fi} is the energy gap between the final state and initial state, and ω is the excitation photon frequency. $\vec{\mu}_{mi}$ is the transition dipole moment between the initial state and the intermediate state, $\vec{\mu}_{fm}$ is the transition dipole moment between the intermediate state and the final state, and E_0 is the electric field.

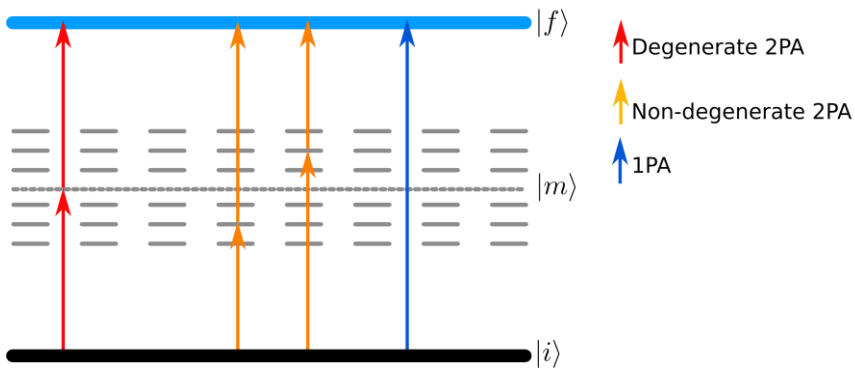

Figure 4.2
Scheme of 2PA energy diagram, an initial state $|i\rangle$ is represented by a black solid line, a manifold of intermediate state $|m\rangle$ is represented by gray dashed lines, and a final state $|f\rangle$ is represented by a blue solid line.

The intermediate state can be either a virtual state or a real state with negligible single-photon absorption. Such sub-band gap states are present in conventional CdSe NCs, because the defect/trap states from nonbonding or weakly bonding atoms are located deeply in the band gap.[31, 36, 102] However, this is not the case for $CsPbBr_3$ NCs. In $CsPbBr_3$ perovskite, the same as other LHPs, the band gap is formed between two sets of anti-bonding orbitals.[31] Hence, the defect/trap states are formed within the conduction or valence band, or they form so-called shallow defects, which are close to the conduction band edge.[36, 41] This ensures that $CsPbBr_3$ NCs are defect-tolerant and show high PLQY (up to 90%)[22]. This suggests that the intermediate state is a virtual state in the 2PA process in $CsPbBr_3$ NCs. Moreover, this argument can be further verified by the excitation intensity-dependent PL intensity: 2PA via a virtual state leads to quadratic dependence of two photon-excited PL intensity on excitation intensity; if 2PA occurs via a defect/trap state, subquadratic power dependence appears.[103] In $CsPbBr_3$ NCs, a quadratic dependence has been reported.[76, 96] This indicates that the 2PA occurs via a virtual state.

The final state can be either an exciton or a defect/trap state. The nature of the finial state can be identified from the size dependence of the 2PA cross section $\sigma^{(2)}$. Chou et al.[104] have calculated the size dependence of $\sigma^{(2)}$ by using a simple model: A large number of interaction units were used to represent the NC volume. The Hückel approach was utilized to describe the exciton states of the system.[104] They found that if the final state is an exciton state, then $\sigma^{(2)}$ shows a third-order power-law dependence on the NCs size, whereas $\sigma^{(2)}$ shows a sixth-order power-law dependence on the size if the final state is a nonexcitonic defect state.[76, 104] In this work, we used the TA spectroscopy method to measure $\sigma^{(2)}$ of $CsPbBr_3$ NCs with five different sizes. $\sigma^{(2)}$ increases with NC size following a power-law dependence with exponent 3.3 (Figure 4.3a). This is close to the third-order power-law dependence, and a small deviation can be present due to the approximations used in the theoretical model.[104] Hence, we can assign the final state to an exciton state. This is further supported by the fact that $\sigma^{(2)}$ follows well the trend of the 1PA cross section (Figure 4.3b). Here, we conclude that the 2PA process in $CsPbBr_3$ NCs proceeds through a virtual level and the final state is an exciton band state and not a defect state.

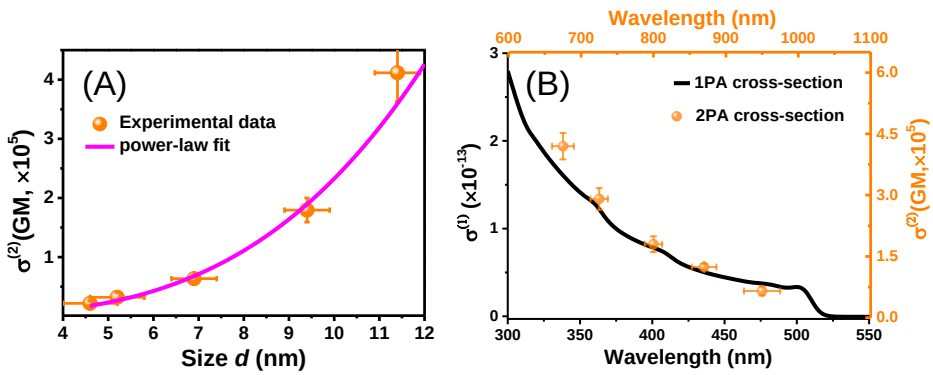

Figure 4.3
(a) $\sigma^{(2)}$ of NCs with different sizes and the data are fitted by using a power-law function ($\sigma^{(2)} = Cd^{\alpha}$,C=111±55, α = 3.3 ±0.2). (b) Wavelength-dependent absorption cross sections of the 9.4 nm size NCs. Black line, 1PA cross section $\sigma^{(1)}$, Yellow dots, TPA cross section $\sigma^{(2)}$ (1 GM corresponds to 10^{-50} cm^4 s/photon) at 675 nm, 725 nm, 800 nm, 870 nm and 950 nm.

4.3 Enhanced Size Selection in Two-Photon Excitation for $CsPbBr_3$ Nanocrystals

If the origin of different PL emission and decay is due to the different excited states accessed by 2PA and 1PA, we would expect different state-specific features appearing in TA spectra for 2PA and 1PA excitation. But this is not the case here.

The TA spectra show the same spectral behaviour with 2PA and 1PA from 5 ps to 3 ns (Figure 4.4a). Although, different states can be accessed by 2PA and 1PA because of different selection rules, these states undergo a rapid cooling (~ps) and relax to the same lowest excited state. Hence, we can rule out the possibility that different states induce the differences in PL emission. On the other hand, PL spectra, as well as PL and TA kinetics show size-dependence (see Figure 4.4b-d).[29] The 2PA cross section shows a stronger size-dependence compared to the 1PA cross section. Therefore, the larger NCs can be preferably excited under 2PA. We conclude that size inhomogeneity (see Figure 4.4e) is the reason for the red-shifted PL spectrum, relatively slow TRPL and TA kinetics with two-photon excitation. Furthermore, we simulated PL emission with 2PA and 1PA based on size-dependent PL emission (Figure 4.4d) and the NC size distribution from TEM (Figure 4.4e). A clear red-shift can be observed in the simulated 2PA- and 1PA-induced PL spectra (see Figure 4.4f). The simulations agree well with the experimental results supporting our conclusion that the differences between the excited state dynamics after 2PA and 1PA excitation in $CsPbBr_3$ NCs are due to the different size selection by the excitation under these two conditions.

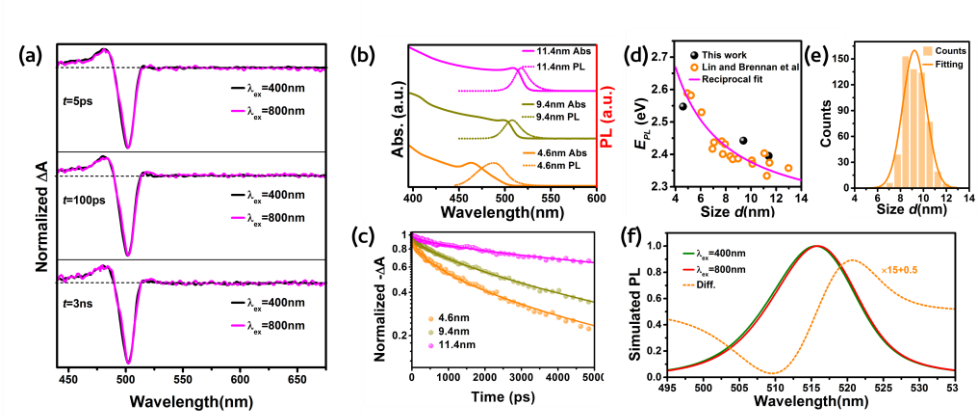

Figure 4.4
(a) TA spectra of $CsPbBr_3$ NCs with size d=9.4 nm at different delay time with 400 nm and 800 nm excitation; (b) Absorption and PL spectra (λ_{ex}= 400 nm) of $CsPbBr_3$ NCs with different sizes; (c) TA kinetics for $CsPbBr_3$ NCs with three different sizes with 400 nm weak excitation; (d) size-dependent PL emission energy (E_{PL}) data points from this work (black balls), calculated based on literature data from Lin et al.[105] and Brennan et al.[106] (open orange circles), fit to the data points by $E_{PL}=E_0 + A/d$ (orange curve, E_0=2.2eV, A=2.0(eV•nm); (e) The size distribution histograms of $CsPbBr_3$ NCs (d=9.4 nm) measured along all edges; (f) Simulated PL emission with 400 nm (blue curve) and 800 nm (red curve) excitation, the simulated (orange dashed curve) difference (Diff.) between two- and one-photon excited PL spectra.

4.4 Refinement of the Size-Dependent Two-Photon Absorption Cross Section

As we discussed in section 4.3, under 2PA larger NCs are preferably excited. The actual size of 2PA-excited NCs in Figure 4.3a should be slightly larger than the value from TEM statistical analysis, which might induce a different size-dependent 2PA cross section. To verify this, we estimated that the size difference (Δd) is about 1 nm, 0.2 nm and 0 nm for NCs with d=4.6, 9.4 and 11.4 nm, respectively. The estimation was based on the measured PL emission under one- and two-photon excitation (Figure 4.5a) and size-dependent PL emission energy (Figure 4.4d). We can calculate Δd for other NCs by using a linear function ($\Delta d = 1.68 - 0.15d$), which is obtained by fitting these Δd values for NCs with d=4.6, 9.4 and 11.4 nm. Figure 4.5b shows the size-dependent 2PA cross section with corrected actual two photon-excited NC size ($d' = \Delta d + d$). $\sigma^{(2)}$ increases with NCs size following a power-law dependence with exponent 4.0. This result is somewhat larger than the value (3.3) in section 4.2 and would not change the conclusion that the 2PA process in $CsPbBr_3$ NCs proceeds through a virtual level and the final state is an exciton band state and not a defect state, which we have discussed above.

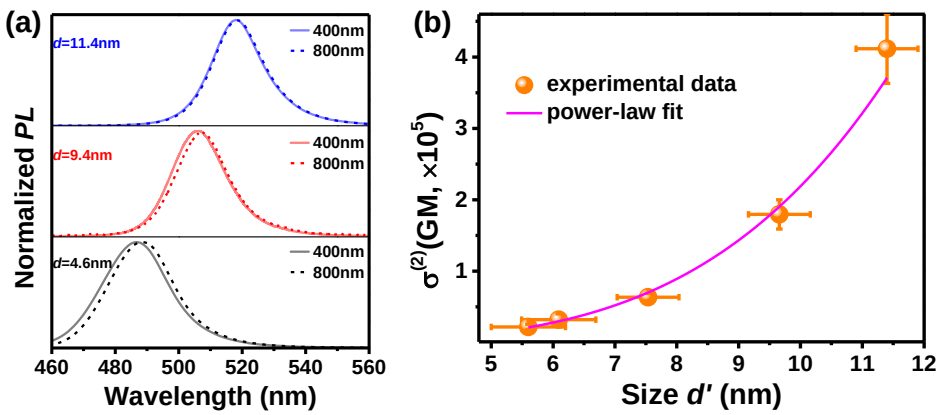

Figure 4.5
(a) PL spectra of $CsPbBr_3$ NCs with different sizes under 400 nm and 800 nm excitation; (b) $\sigma^{(2)}$ of NCs with different sizes (actual two-photon excited NCs size d') and the data are fitted by using a power-law function ($\sigma^{(2)} = Cd'^{\alpha}$,C=21 ±7, α = 4.0±0.2).

Chapter 5: Lead Halide Perovskite Microcrystals for Photodetector Applications

Radiative recombination of charge carriers is the primary process behind LED and laser applications. In an opposite process, the photogenerated charge carriers should be separated and extracted. Efficient charge carrier separation and transportation are important for solar-cell and photodetector systems.[107] However, the long-chained surface capping ligands on NCs will hinder the intercrystal charge transportation in the conventional compacted NCs assembly, and lead to a poor performance in these kinds of devices. In this scenario, ligand exchange to shorten the intercrystal spacing is necessary. However, as we discussed in section 1.2.3, neither centimeter/millimeter sized single crystals nor films is the best candidate for studying the intrinsic photophysics in these devices, as the size is much larger than the diffusion length of charge carriers or carrier transport is hindered by grain boundaries. In paper IV, we use micrometer-sized $CsPbBr_3$ single crystals to fabricate photodetectors, and study the photophysics in these single crystals and devices.

5.1 Photodetectors based on Lead Halide Perovskite Microcrystals

5.1.1 Photodetector Schemes based on Lead Halide Perovskite Crystals

There are different types of photodetectors, with different operation principles, such as photo-voltaic type and photoconductor type.[108] In this thesis, we just focus on photoconductor type photodetectors. As shown in Figure 5.1a, single crystal based photodetectors can be fabricated based on large size (mm~cm) crystals.[109-110] However, the typical size of the crystals is up to a millimeter or centimeter. It is several orders of magnitudes larger than the diffusion length of charge carriers in LHP materials (~several μm). This can increase the possibility for the charge

carriers to be trapped before they reach the electrodes. The performance of the devices might be diminished due to trapping or other processes in the large crystals.

In this work, we deposited LHP MCs on a planar glass substrate with two ITO electrodes (with 5 μm channel width and 1000 μm length, see Figure 5.1b). It has been reported that these crystalline films show mobility and diffusion length comparable with mm-size single crystals.[69] Due to the fact that the size of the active material is comparable to the diffusion length, the charge carriers can be collected efficiently. Hence, the microcrystal layer-based photodetector devices show high performance.

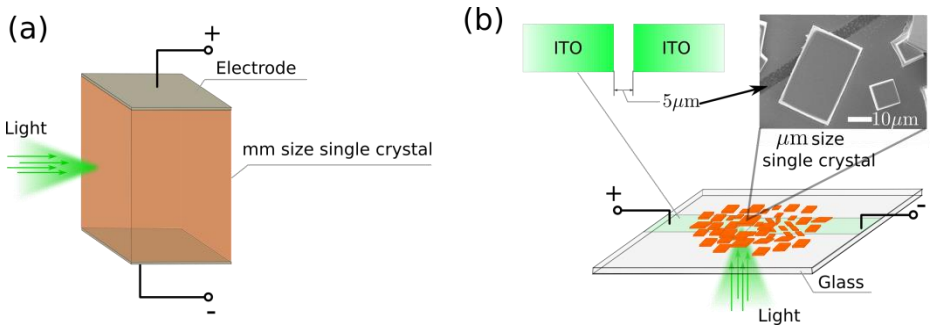

Figure 5.1
Photoconductor type photodetector schemes: (a) based on a mm-size LHP single crystal; (b) based on a μm-size LHP single crystals.

5.1.2 Basic Important Parameters of Photodetectors

There are many different parameters which determine the performance of a photodetector. The scope of this thesis is mainly focused on photophysics. Here we briefly introduce several important properties of photodetectors.

The responsivity (R) is a performance parameter for photodetectors. It defines the magnitude of the output electric signal from a photodetector in response to a particular light power:[111]

$$R(\lambda) = \frac{I_{PD}}{P(\lambda)} \qquad (5.1)$$

In which λ is the wavelength of the light, I_{PD} is the photocurrent output from the photodetector (unit: A), and $P(\lambda)$ is the incident light power (unit: W) for light with wavelength λ.

The external quantum efficiency (EQE) is defined as the ratio between the number of electrons in the external circuit and the number of photons absorbed by the active material in a photodetector.

$$\mathrm{EQE}(\lambda) = \frac{R(\lambda)\cdot hc}{q\lambda} \qquad (5.2)$$

Here, h is Planck's constant, c is the speed of light and q is the elementary charge.

The detectivity (D^*) of a photodetector can be calculated based on the dark current (I_{dark}), R and the active area of the detector (A):[111]

$$D^* = \frac{R\sqrt{A}}{\sqrt{qI_{dark}}} \qquad (5.3)$$

The photoconductive gain (G) is defined as the ratio between the output current and the current directly produced by the photons impinging on the detector. It can also be calculated based on the ratio between charge lifetime (τ_1, the lifespan of the charge in the photodetector circuit) and charge transit time (τ_t, the charge transport time in the photodetector circuit).[69, 112] G can be increased by trapping one type of the charge carriers, and the life time of another type of charge carriers can be extended.[112]

$$G = \frac{\tau_1}{\tau_t} \qquad (5.4)$$

Here τ_1 is given by the response time: rise time (τ_r) and fall time (τ_f) of the photodetectors. The rise (fall) time is defined as the time for the signal to rise (fall) from 10% (90%) to 90% (10%) of the final value.[69, 113] τ_t is the charge carrier transit time, which is inversely proportional to the mobility (μ) of the charge carrier:[69]

$$\tau_t = \frac{L^2}{V\mu} \qquad (5.5)$$

Here, L is the sample active length and V is the applied voltage.

The electrical bandwidth (f_{3db}) can be roughly approximated by:[113]

$$f_{3db} \cong \frac{1}{\tau_r} \qquad (5.6)$$

By multiplying the gain and the electrical band-width, we can obtain the gain-bandwidth product~Gf_{3db}.

We fabricated photodetectors (see Figure 5.1b) based on a layer of $CsPbBr_3$ MCs with high performance. The high performance results from efficient charge carrier collection and the intrinsic properties of the MCs, such as the large absorption coefficient, high charge carrier mobility and the low trap-state density.

5.2 $CsPbBr_3$ Microcrystals for Near-Infrared Light Detection

For conventional photodetectors, the energy of the detected light has to be larger than or equal to the band gap energy of the active material in the photodetectors. As we discussed in chapter 4, $CsPbBr_3$ LHP NCs show strong 2PA. Here we find that $CsPbBr_3$ LHP MCs show the 2PA process and the MC layer-based photodetectors can be applied for detecting NIR pulsed laser light with energy below the band gap of $CsPbBr_3$ crystals. Such NIR detectors can be used for detecting the intensity of high-power pulsed NIR laser.

Similar to $CsPbBr_3$ NCs, different PL emission spectra are observed for 1PA and 2PA in $CsPbBr_3$ MCs. 1PA-induced PL shows a double-peak PL emission (520 and 545 nm). On the other hand, a single peak (545 nm) is present in 2PA-induced PL emission. The different PL emission can be ascribed to the different charge carrier dynamic processes under 1PA and 2PA. 1PA-generated charge carriers are mostly located at the surface of MCs, due to the limited penetration depth of light. The charge carriers are ready to recombine radiatively or diffuse from the surface into the NCs. The two different processes lead to two different PL emission peaks. However, under 2PA, NIR light has a longer penetration depth compared to the UV–Vis light in 1PA. In this case, the charge carriers are generated in the MCs and reabsorption plays an important role, leading to the single band red-shifted PL emission and increased PL lifetime.

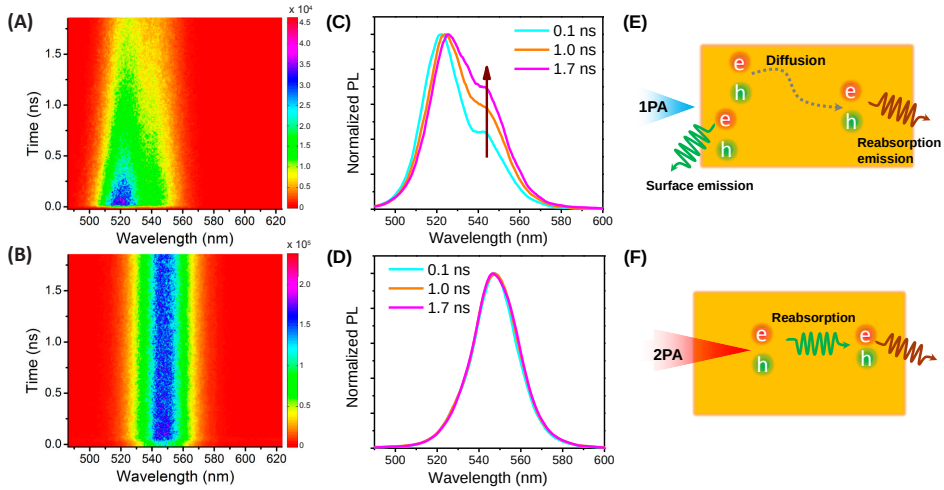

Figure 5.2
Time-resolved PL spectra under a) 1PA (λ_{ex}=410 nm) and b) 2PA (λ_{ex}=800 nm) of $CsPbBr_3$ MCs. c) PL spectra at different delay time under 1PA. d) PL spectra at different delay time under 2PA. e) and f) Schematic diagram of carrier diffusion and recombination processes with 1PA and 2PA, respectively.

Chapter 6: Photophysics in Lead Free Caesium Bismuth Halide Perovskite Nanocrystals

The success of LHP materials for solar-cell, LED and display applications has naturally led to both extensive fundamental and application oriented research. However, there are still a number of obstacles preventing the commercialization of LHP materials, such as long-term stability and toxicity. Especially the toxic lead element in conventional LHP materials pose a threat to the environment and can harm living organisms. Therefore, it is difficult to legislate lead-based perovskite materials in the European Union (EU) that are regulated by RoHS (Restriction of Hazardous Substances, Directive 2011/65/EU of the European Parliament).[31, 114] Extensive experimental and theoretical works were initiated to find metal halide compounds with alternative environmentally friendly elements with comparable photophysical properties. Many different metal elements have been introduced into perovskite structures, such as Sb, Bi, Ag, Cu, In, Mn et al.[31] However, it is challenging to obtain lead-free perovskite materials with as good optical and electronic properties as LHPs. Therefore, it is urgent to understand the photophysics in these lead-free perovskite compounds. In this work, we used less toxic bismuth[115] as a replacement of lead to synthesize caesium bismuth halide perovskite $Cs_3Bi_2X_9$ (X=Cl, Br, I) NCs and we studied their photophysics.

6.1 $Cs_3Bi_2X_9$ Nanocrystal Synthesis

$Cs_3Bi_2X_9$ NCs were synthesized by the anti-solvent precipitation crystallization method, which has been described in chapter 2. Briefly, Cs halides and Bi halides were dissolved in DMSO and a precursor solution was formed. A small amount of the precursor solution was injected into the anti-solvent 2-propanol. $Cs_3Bi_2X_9$ NCs were formed instantly (within 30 seconds). Figure 6.1a shows the as-synthesized colloidal $Cs_3Bi_2X_9$ NCs. TEM was used to characterize the NCs. As shown in Figure 6.1b, the $Cs_3Bi_2X_9$ NCs exhibited a quasi-spherical shape with 6 nm diameter.

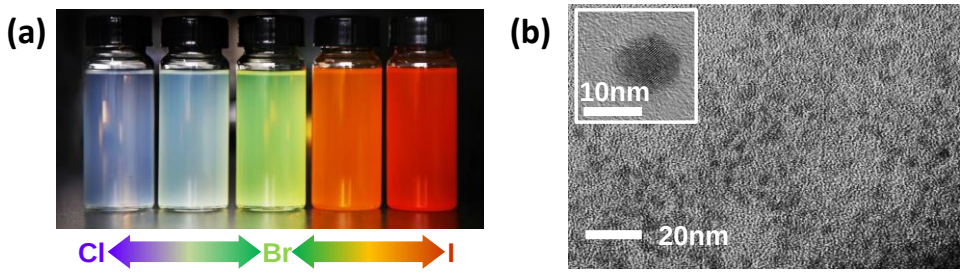

Figure 6.1
a). Photographs of as-synthesized colloidal $Cs_3Bi_2X_9$ (X=Cl, $Cl_{0.5}Br_{0.5}$, Br, $Br_{0.5}I_{0.5}$, I); b). TEM image of $Cs_3Bi_2Br_9$ NCs, inset: high resolution TEM image.

The crystal structure of $Cs_3Bi_2X_9$ is different from that of conventional ABX_3 perovskite as shown in chapter 1. The unit cell and crystal structure of $Cs_3Bi_2Br_9$ are illustrated in Figure 6.2. An octahedron unit is formed by the metal cation Bi^{3+} and anion Br^- ions (see Figure 6.2). Different from the formation of a framework by sharing the corner of BX_6 octahedron in ABX_3 perovskite structure, metal halide octahedral layers are formed in $Cs_3Bi_2Br_9$ (see Figures 1.1 and 6.2b) and the voids between the layers are filled with Cs^+ cations.[116]

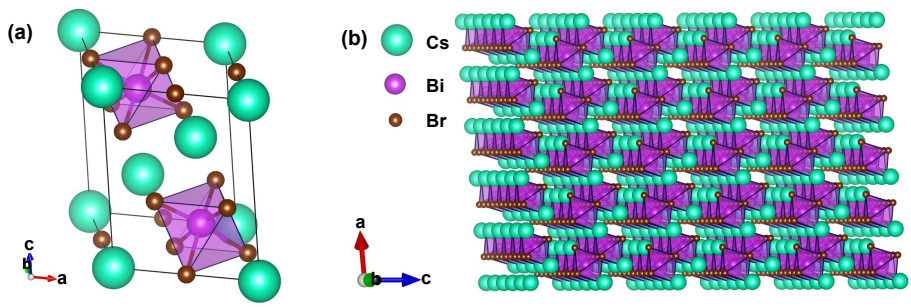

Figure 6.2
Crystal structure of $Cs_3Bi_2Br_9$, (a) Unit cell of $Cs_3Bi_2Br_9$, (b) 3-dimensional lattice structure

6.2 Photoluminescence of $Cs_3Bi_2X_9$ NCs

The PL emission peak of $Cs_3Bi_2X_9$ NCs can be tuned from 400 to 560 nm by changing the halide composition. However, they show very low PL emission intensity. Their PLQY is two orders of magnitude lower than that of $CsPbX_3$ NCs (see Table 6.1). With such low PLQY, it is difficult to use $Cs_3Bi_2X_9$ NCs for lighting applications.

Table 6.1
PLQY of $Cs_3Bi_2X_9$ and $CsPbX_3$ NCs[a]

X	Cl	($Cl_{0.5}/Br_{0.5}$)	Br	($Br_{0.5}/I_{0.5}$)	I
Ligand Free	0.1%	0.1%	0.2%	<0.1%	<0.1%
OA capped	0.1%	0.3%	4.5%	<0.1%	<0.1%
$CsPbX_3$	10%	37%	95%	72%	70%

[a]Data is taken from Li et al.[117]

Many reasons can lead to such low PLQY and one of the reasons can be the dangling bonds on the NC surface. Here we try to cap the NC surface with OA during the synthesis (see section 2.1.1). The PLQY of $Cs_3Bi_2Br_9$ is increased from 0.2% to 4.5% by capping the NCs with OA (see Table 6.1 and Figure 6.3), whereas, OA shows negligible influence on other halide $Cs_3Bi_2X_9$ NCs.

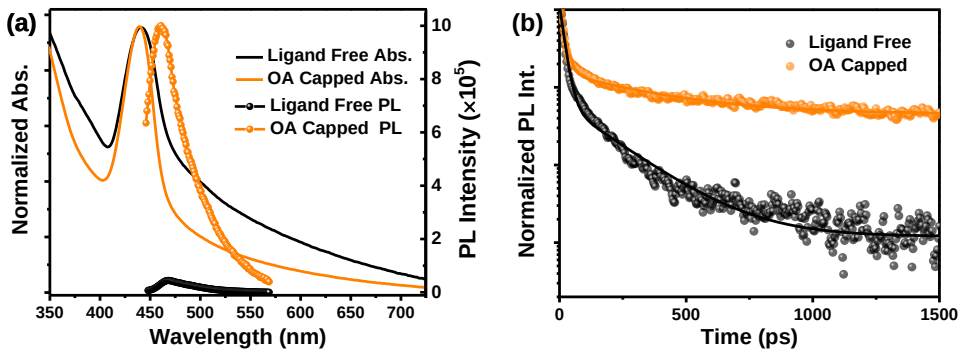

Figure 6.3
(a): Absorption and PL spectra of ligand-free $Cs_3Bi_2X_9$ NCs and OA-capped $Cs_3Bi_2X_9$ NCs. The absorption spectra have been taken in an integrating sphere-coupled absorption spectrometer; (b): TRPL kinetics of ligand-free NCs and OA-capped NCs measured with streak camera (λ_{ex}=400 nm).

As shown in Figure 6.3a, an absorption tail up to 700 nm is present in the absorption spectrum. A similar absorption tails have been reported in $MAPbBr_3$ NCs and $MAPbI_3$ films, where they were assigned to trap-state absorption.[118-119] The absorption tail is suppressed for OA-capped NCs. The suppressed absorption tail and the increased PLQY indicate that the trap states are partly passivated by OA. OA-capped NCs show slower PL decay compared with ligand-free NCs. This further supports that trap states are passivated.

However, the OA-capped NCs still show low PLQY (4.5%), and this is not comparable with $CsPbX_3$ NCs. In order to understand the photophysics of the low PLQY, we carried out TA experiments. The TA spectrum is shown in Figure 6.4a. By analysing the TA kinetics, we find that there is still a fast trapping pathway present (see Figure 6.4b), which competes with radiative band-edge recombination. This leads to a low PLQY even in OA-capped $Cs_3Bi_2Br_9$ NCs.

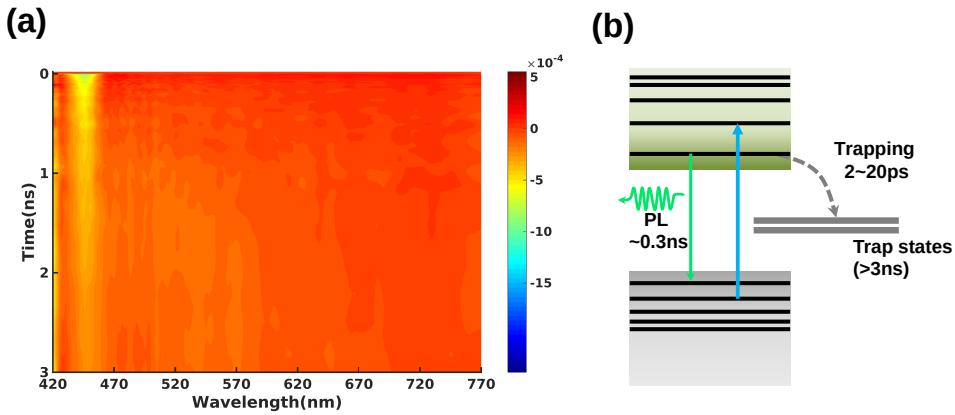

Figure 6.4
(a): TA spectra of OA-capped $Cs_3Bi_2Br_9$ NCs (λ_{ex}=400 nm); b) Excited-state dynamics model of $Cs_3Bi_2Br_9$ NCs.

Chapter 7: Conclusion

In this work, we have studied the photophysics of perovskite NCs and MCs by using different spectroscopic methods. These results can be important for both fundamental research and applications in devices.

$CsPbBr_3$ NCs demonstrate promising potential in LED and display applications. However, the material stability becomes a critical factor that needs to be considered. In this work we studied the stability of as-synthesized $CsPbBr_3$ NCs suspended in toluene at different storage conditions (temperature, atmosphere and light irradiation). We found that the stability of $CsPbBr_3$ NCs is very sensitive to the irradiation, which induces aggregation of the NCs, leading to the formation of larger crystals. This indicates that proper NCs surface modification is needed for the application of $CsPbBr_3$ NCs.

$CsPbBr_3$ NCs show red-shifted PL emission and increased PL lifetime under 2PA compared to 1PA-induced PL emission. In order to understand the photophysics behind this, we studied the 2PA process in $CsPbBr_3$ NCs by measuring the 2PA cross-section of $CsPbBr_3$ NCs with different sizes. We found that the 2PA cross section of $CsPbBr_3$ NCs shows size- and wavelength- dependence. The 2PA cross section has third-order power-law size dependence and follows the 1PA cross section wavelength dependence. This allows us to assign the final state of 2PA to an exciton state. Furthermore, we observed that the 2PA cross section exhibits stronger size dependence than that in the 1PA cross section. As a result, larger NCs are preferably excited. This leads to red-shifted PL emission and longer excited-state lifetime.

LHP MCs show low trap density, high charge carrier mobility and long diffusion length. Especially the size of the MCs is close to the diffusion length and this enables efficient charge carrier collection. We fabricated $CsPbBr_3$ MCs layer-based photodetectors, which show high responsivity, and fast response in both the visible region (the 1PA process) and the NIR region (the 2PA process). Furthermore, we found that depending on the excitation conditions, $CsPbBr_3$ MCs show different PL emission spectra: double and single-peak PL emission is observed under 1PA and 2PA, respectively. Time resolved spectra indicate that the different PL emission is due to the fact that 1PA light (visible-range) has shorter penetration depth than 2PA light (NIR). Charge carriers are generated at different

positions of the MCs, and this leads to different charge carrier dynamic processes under 1PA and 2PA.

The toxic lead-based materials pose a threat to the environment and living organisms, which is an obstacle for the commercialization of LHP materials. Here, we replaced the lead element with less toxic bismuth in perovskite NCs. The emission of $Cs_3Bi_2X_9$ NCs can be tuned from 400 to 560 nm by changing the halide composition. However, they exhibit very low PL emission intensity compared with $CsPbX_3$ NCs. The PL emission of $Cs_3Bi_2Br_9$ NCs can be increased from 0.2% to 4.5% by surface passivation with OA. We investigated the reason for the low PL emission of $Cs_3Bi_2Br_9$ NCs by using time-resolved spectroscopy and found that there is a fast non-radiative trapping process, which competes with radiative decay and leads to the low PL emission intensity.

References

1. Dusastre, V.; Martiradonna, L. Materials for sustainable energy. *Nature Materials* **2017,** *16*, 15-15.

2. Chu, S.; Cui, Y.; Liu, N. The path towards sustainable energy. *Nature Materials* **2017,** *16*, 16-22.

3. Boot-Handford, M. E.; Abanades, J. C.; Anthony, E. J.; Blunt, M. J.; Brandani, S.; Mac Dowell, N.; Fernandez, J. R.; Ferrari, M. C.; Gross, R.; Hallett, J. P.; Haszeldine, R. S.; Heptonstall, P.; Lyngfelt, A.; Makuch, Z.; Mangano, E.; Porter, R. T. J.; Pourkashanian, M.; Rochelle, G. T.; Shah, N.; Yao, J. G.; Fennell, P. S. Carbon capture and storage update. *Energy & Environmental Science* **2014,** *7*, 130-189.

4. Cho, J.; Park, J. H.; Kim, J. K.; Schubert, E. F. White light-emitting diodes: History, progress, and future. *Laser & Photonics Reviews* **2017,** *11*, 1600147.

5. Green, M. A.; Hishikawa, Y.; Warta, W.; Dunlop, E. D.; Levi, D. H.; Hohl-Ebinger, J.; Ho-Baillie, A. W. Y. Solar cell efficiency tables (version 50). *Progress in Photovoltaics* **2017,** *25*, 668-676.

6. https://www.nrel.gov/pv/assets/images/efficiency-chart.png.

7. Yang, W. S.; Park, B. W.; Jung, E. H.; Jeon, N. J.; Kim, Y. C.; Lee, D. U.; Shin, S. S.; Seo, J.; Kim, E. K.; Noh, J. H.; Seok, S. I. Iodide management in formamidinium-lead-halide-based perovskite layers for efficient solar cells. *Science* **2017,** *356*, 1376–1379.

8. Yang, S. D.; Fu, W. F.; Zhang, Z. Q.; Chen, H. Z.; Li, C. Z. Recent advances in perovskite solar cells: efficiency, stability and lead-free perovskite. *Journal of Materials Chemistry A* **2017,** *5*, 11462-11482.

9. Wang, H.; Kim, D. H. Perovskite-based photodetectors: materials and devices. *Chemical Society Reviews* **2017,** *46*, 5204-5236.

10. Wei, H. T.; Fang, Y. J.; Mulligan, P.; Chuirazzi, W.; Fang, H. H.; Wang, C. C.; Ecker, B. R.; Gao, Y. L.; Loi, M. A.; Cao, L.; Huang, J. S. Sensitive X-ray

detectors made of methylammonium lead tribromide perovskite single crystals. *Nature Photonics* **2016,** *10*, 333-339.

11. Zhang, Q.; Su, R.; Du, W. N.; Liu, X. F.; Zhao, L. Y.; Ha, S. T.; Xiong, Q. H. Advances in Small Perovskite-Based Lasers. *Small Methods* **2017,** *1*, 1700163.

12. Pietryga, J. M.; Park, Y. S.; Lim, J. H.; Fidler, A. F.; Bae, W. K.; Brovelli, S.; Klimov, V. I. Spectroscopic and Device Aspects of Nanocrystal Quantum Dots. *Chemical Reviews* **2016,** *116*, 10513-10622.

13. Matthews, P. D.; Lewis, D. J.; O'Brien, P. Updating the road map to metal-halide perovskites for photovoltaics. *Journal of Materials Chemistry A* **2017,** *5*, 17135-17150.

14. Ali, R.; Yashima, M. Space group and crystal structure of the Perovskite CaTiO3 from 296 to 1720K. *Journal of Solid State Chemistry* **2005,** *178*, 2867-2872.

15. Lufaso, M. W.; Woodward, P. M. Prediction of the crystal structures of perovskites using the software program SPuDS. *Acta Crystallographica Section B-Structural Science* **2001,** *57*, 725-738.

16. Poglitsch, A.; Weber, D. Dynamic Disorder in Methylammoniumtrihalogenoplumbates(Ii) Observed by Millimeter-Wave Spectroscopy. *Journal of Chemical Physics* **1987,** *87*, 6373-6378.

17. Gratzel, M. The Rise of Highly Efficient and Stable Perovskite Solar Cells. *Accounts of Chemical Research* **2017,** *50*, 487-491.

18. *CsPbBr3 Crystal Structure: Datasheet from "PAULING FILE Multinaries Edition – 2012" in SpringerMaterials (http://materials.springer.com/isp/crystallographic/docs/sd_0545372)*, Springer-Verlag Berlin Heidelberg & Material Phases Data System (MPDS), Switzerland & National Institute for Materials Science (NIMS), Japan.

19. Merdasa, A. Super-resolution Luminescence Micro-Spectroscopy : A nano-scale view of solar cell material photophysics. Lund University, Lund, 2017.

20. Koscher, B. A.; Swabeck, J. K.; Bronstein, N. D.; Alivisatos, A. P. Essentially Trap-Free CsPbBr3 Colloidal Nanocrystals by Postsynthetic Thiocyanate Surface Treatment. *Journal of the American Chemical Society* **2017,** *139*, 6566-6569.

21. Schmidt, L. C.; Pertegas, A.; Gonzalez-Carrero, S.; Malinkiewicz, O.; Agouram, S.; Espallargas, G. M.; Bolink, H. J.; Galian, R. E.; Perez-Prieto, J.

Nontemplate Synthesis of CH3NH3PbBr3 Perovskite Nanoparticles. *Journal of the American Chemical Society* **2014,** *136*, 850-853.

22. Protesescu, L.; Yakunin, S.; Bodnarchuk, M. I.; Krieg, F.; Caputo, R.; Hendon, C. H.; Yang, R. X.; Walsh, A.; Kovalenko, M. V. Nanocrystals of Cesium Lead Halide Perovskites (CsPbX(3), X = Cl, Br, and I): Novel Optoelectronic Materials Showing Bright Emission with Wide Color Gamut. *Nano Letters* **2015,** *15*, 3692-3696.

23. Zheng, K. B.; Zhu, Q. S.; Abdellah, M.; Messing, M. E.; Zhang, W.; Generalov, A.; Niu, Y. R.; Ribaud, L.; Canton, S. E.; Pullerits, T. Exciton Binding Energy and the Nature of Emissive States in Organometal Halide Perovskites. *Journal of Physical Chemistry Letters* **2015,** *6*, 2969-2975.

24. De Roo, J.; Ibanez, M.; Geiregat, P.; Nedelcu, G.; Walravens, W.; Maes, J.; Martins, J. C.; Van Driessche, I.; Koyalenko, M. V.; Hens, Z. Highly Dynamic Ligand Binding and Light Absorption Coefficient of Cesium Lead Bromide Perovskite Nanocrystals. *Acs Nano* **2016,** *10*, 2071-2081.

25. Zhu, Q. S.; Zheng, K. B.; Abdellah, M.; Generalov, A.; Haase, D.; Carlson, S.; Niu, Y. R.; Heimdal, J.; Engdahl, A.; Messing, M. E.; Pullerits, T.; Canton, S. E. Correlating structure and electronic band-edge properties in organolead halide perovskites nanoparticles. *Physical Chemistry Chemical Physics* **2016,** *18*, 14933-14940.

26. Zhang, F.; Zhong, H. Z.; Chen, C.; Wu, X. G.; Hu, X. M.; Huang, H. L.; Han, J. B.; Zou, B. S.; Dong, Y. P. Brightly Luminescent and Color-Tunable Colloidal CH3NH3PbX3 (X = Br, I, Cl) Quantum Dots: Potential Alternatives for Display Technology. *Acs Nano* **2015,** *9*, 4533-4542.

27. Yang, Z.; Surrente, A.; Galkowski, K.; Miyata, A.; Portugall, O.; Sutton, R. J.; Haghighirad, A. A.; Snaith, H. J.; Maude, D. K.; Plochocka, P.; Nicholas, R. J. Impact of the Halide Cage on the Electronic Properties of Fully Inorganic Cesium Lead Halide Perovskites. *Acs Energy Letters* **2017,** *2*, 1621-1627.

28. Aneesh, J.; Swarnkar, A.; Ravi, V. K.; Sharma, R.; Nag, A.; Adarsht, K. V. Ultrafast Exciton Dynamics in Colloidal CsPbBr3 Perovskite Nanocrystals: Biexciton Effect and Auger Recombination. *Journal of Physical Chemistry C* **2017,** *121*, 4734-4739.

29. Shinde, A.; Gahlaut, R.; Mahamuni, S. Low-Temperature Photoluminescence Studies of CsPbBr3 Quantum Dots. *Journal of Physical Chemistry C* **2017,** *121*, 14872–14878.

30. Li, J.; Luo, L. H.; Huang, H. W.; Ma, C.; Ye, Z. Z.; Zeng, J.; He, H. P. 2D Behaviors of Excitons in Cesium Lead Halide Perovskite Nanoplatelets. *Journal of Physical Chemistry Letters* **2017,** *8*, 1161-1168.

31. Kovalenko, M. V.; Protesescu, L.; Bodnarchuk, M. I. Properties and potential optoelectronic applications of lead halide perovskite nanocrystals. *Science* **2017,** *358*, 745-750.

32. Brus, L. E. Electron Electron and Electron-Hole Interactions in Small Semiconductor Crystallites - the Size Dependence of the Lowest Excited Electronic State. *Journal of Chemical Physics* **1984,** *80*, 4403-4409.

33. Brandt, R. E.; Stevanovic, V.; Ginley, D. S.; Buonassisi, T. Identifying defect-tolerant semiconductors with high minority-carrier lifetimes: beyond hybrid lead halide perovskites. *Mrs Communications* **2015,** *5*, 265-275.

34. Madlet, M. E.; Berdiyorov, G. R.; El-Mellouhi, F.; Alharbi, F. H.; Akimov, A. V.; Kais, S. Cation Effect on Hot Carrier Cooling in Halide Perovskite Materials. *Journal of Physical Chemistry Letters* **2017,** *8*, 4439-4445.

35. Chung, H.; Il Jung, S.; Kim, H. J.; Cha, W.; Sim, E.; Kim, D.; Koh, W. K.; Kim, J. Composition-Dependent Hot Carrier Relaxation Dynamics in Cesium Lead Halide (CsPbX3, X = Br and I) Perovskite Nanocrystals. *Angewandte Chemie-International Edition* **2017,** *56*, 4160-4164.

36. Brandt, R. E.; Poindexter, J. R.; Gorai, P.; Kurchin, R. C.; Hoye, R. L. Z.; Nienhaus, L.; Wilson, M. W. B.; Polizzotti, J. A.; Sereika, R.; Zaltauskas, R.; Lee, L. C.; MacManus-Driscoll, J. L.; Bawendi, M.; Stevanovic, V.; Buonassisi, T. Searching for "Defect-Tolerant" Photovoltaic Materials: Combined Theoretical and Experimental Screening. *Chemistry of Materials* **2017,** *29*, 4667-4674.

37. Rabouw, F. T.; Donega, C. D. Excited-State Dynamics in Colloidal Semiconductor Nanocrystals. *Topics in Current Chemistry* **2016,** *Z*, 374: 58.

38. Klimov, V. I.; McBranch, D. W. Femtosecond 1P-to-1S electron relaxation in strongly confined semiconductor nanocrystals. *Physical Review Letters* **1998,** *80*, 4028-4031.

39. Geiregat, P.; Delerue, C.; Justo, Y.; Aerts, M.; Spoor, F.; Van Thourhout, D.; Siebbeles, L. D. A.; Allan, G.; Houtepen, A. J.; Hens, Z. A Phonon Scattering Bottleneck for Carrier Cooling in Lead Chalcogenide Nanocrystals. *Acs Nano* **2015,** *9*, 778-788.

40. Liu, Q. H.; Wang, Y. H.; Sui, N.; Wang, Y. T.; Chi, X. C.; Wang, Q. Q.; Chen, Y.; Ji, W. Y.; Zou, L.; Zhang, H. Z. Exciton Relaxation Dynamics in Photo-Excited CsPbI3 Perovskite Nanocrystals. *Scientific Reports* **2016,** *6*, 29442.

41. Mondal, N.; Samanta, A. Complete ultrafast charge carrier dynamics in photo-excited all-inorganic perovskite nanocrystals (CsPbX3). *Nanoscale* **2017,** *9*, 1878-1885.

42. Deng, Z. Y.; Guyot-Sionnest, P. Intraband Luminescence from HgSe/CdS Core/Shell Quantum Dots. *Acs Nano* **2016,** *10*, 2121-2127.

43. Diroll, B. T.; Turk, M. E.; Gogotsi, N.; Murray, C. B.; Kikkawa, J. M. Ultrafast Photoluminescence from the Core and the Shell in CdSe/CdS Dot-in-Rod Heterostructures. *Chemphyschem* **2016,** *17*, 759-765.

44. Polman, A.; Atwater, H. A. Photonic design principles for ultrahigh-efficiency photovoltaics. *Nature Materials* **2012,** *11*, 174-177.

45. Nozik, A. J. Spectroscopy and hot electron relaxation dynamics in semiconductor quantum wells and quantum dots. *Annual Review of Physical Chemistry* **2001,** *52*, 193-231.

46. Schaller, R. D.; Klimov, V. I. High efficiency carrier multiplication in PbSe nanocrystals: Implications for solar energy conversion. *Physical Review Letters* **2004,** *92*, 186601.

47. Sambur, J. B.; Novet, T.; Parkinson, B. A. Multiple Exciton Collection in a Sensitized Photovoltaic System. *Science* **2010,** *330*, 63-66.

48. Beard, M. C.; Luther, J. M.; Semonin, O. E.; Nozik, A. J. Third Generation Photovoltaics based on Multiple Exciton Generation in Quantum Confined Semiconductors. *Accounts of Chemical Research* **2013,** *46*, 1252-1260.

49. Semonin, O. E.; Luther, J. M.; Choi, S.; Chen, H. Y.; Gao, J. B.; Nozik, A. J.; Beard, M. C. Peak External Photocurrent Quantum Efficiency Exceeding 100% via MEG in a Quantum Dot Solar Cell. *Science* **2011,** *334*, 1530-1533.

50. Bohm, M. L.; Jellicoe, T. C.; Tabachnyk, M.; Davis, N. J. L. K.; Wisnivesky-Rocca-Rivarola, F.; Ducati, C.; Ehrler, B.; Bakulin, A. A.; Greenham, N. C. Lead Telluride Quantum Dot Solar Cells Displaying External Quantum Efficiencies Exceeding 120%. *Nano Letters* **2015,** *15*, 7987-7993.

51. Goodwin, H.; Jellicoe, T. C.; Davis, N. J. L. K.; Bohm, M. L. Multiple exciton generation in quantum dot-based solar cells. *Nanophotonics* **2018,** *7*, 111-126.

52. Goppert-Mayer, M. Elementary processes with two quantum transitions. *Annalen Der Physik* **2009,** *18*, 466-479.

53. Kaiser, W.; Garrett, C. G. B. 2-Photon Excitation in Caf2 - Eu2+. *Physical Review Letters* **1961,** *7*, 229.

54. Bhawalkar, J. D.; He, G. S.; Prasad, P. N. Nonlinear multiphoton processes in organic and polymeric materials. *Reports on Progress in Physics* **1996,** *59*, 1041-1070.

55. Cumpston, B. H.; Ananthavel, S. P.; Barlow, S.; Dyer, D. L.; Ehrlich, J. E.; Erskine, L. L.; Heikal, A. A.; Kuebler, S. M.; Lee, I. Y. S.; McCord-Maughon, D.; Qin, J. Q.; Rockel, H.; Rumi, M.; Wu, X. L.; Marder, S. R.; Perry, J. W. Two-photon polymerization initiators for three-dimensional optical data storage and microfabrication. *Nature* **1999,** *398*, 51-54.

56. Zhang, C.; Zhang, F.; Zhu, T.; Cheng, A.; Xu, J.; Zhang, Q.; Mohney, S. E.; Henderson, R. H.; Wang, Y. A. Two-photon-pumped lasing from colloidal nanocrystal quantum dots. *Optics Letters* **2008,** *33*, 2437-2439.

57. Zhou, G.-J.; Wong, W.-Y. Organometallic acetylides of Pt-II, Au-I and Hg-II as new generation optical power limiting materials. *Chemical Society Reviews* **2011,** *40*, 2541-2566.

58. Shen, Y.; Shuhendler, A. J.; Ye, D.; Xu, J. J.; Chen, H. Y. Two-photon excitation nanoparticles for photodynamic therapy. *Chemical Society Reviews* **2016,** *45*, 6725-6741.

59. Di Giacomo, F.; Fakharuddin, A.; Jose, R.; Brown, T. M. Progress, challenges and perspectives in flexible perovskite solar cells. *Energy & Environmental Science* **2016,** *9*, 3007-3035.

60. Moore, D. T.; Sai, H.; Tan, K. W.; Smilgies, D. M.; Zhang, W.; Snaith, H. J.; Wiesner, U.; Estroff, L. A. Crystallization Kinetics of Organic-Inorganic Trihalide Perovskites and the Role of the Lead Anion in Crystal Growth. *Journal of the American Chemical Society* **2015,** *137*, 2350-2358.

61. Bae, W. K.; Char, K.; Hur, H.; Lee, S. Single-step synthesis of quantum dots with chemical composition gradients. *Chemistry of Materials* **2008,** *20*, 531-539.

62. Matteucci, M. E.; Hotze, M. A.; Johnston, K. P.; Williams, R. O. Drug nanoparticles by antisolvent precipitation: Mixing energy versus surfactant stabilization. *Langmuir* **2006,** *22*, 8951-8959.

63. Hong, Y. N.; Lam, J. W. Y.; Tang, B. Z. Aggregation-induced emission. *Chemical Society Reviews* **2011,** *40*, 5361-5388.

64. Ding, J.; Yan, Q. F. Progress in organic-inorganic hybrid halide perovskite single crystal: growth techniques and applications. *Science China Materials* **2017,** *60*, 1063-1078.

65. Ding, J. X.; Zhao, Y.; Du, S. J.; Sun, Y. S.; Cui, H. Z.; Zhan, X. Y.; Cheng, X. H.; Jing, L. Controlled growth of MAPbBr(3) single crystal: understanding the growth morphologies of vicinal hillocks on (100) facet to form perfect cubes. *Journal of Materials Science* **2017,** *52*, 7907-7916.

66. Rakita, Y.; Kedem, N.; Gupta, S.; Sadhanala, A.; Kalchenko, V.; Bohm, M. L.; Kulbak, M.; Friend, R. H.; Cahen, D.; Hodes, G. Low-Temperature Solution-Grown CsPbBr3 Single Crystals and Their Characterization. *Crystal Growth & Design* **2016,** *16*, 5717-5725.

67. Saidaminov, M. I.; Abdelhady, A. L.; Murali, B.; Alarousu, E.; Burlakov, V. M.; Peng, W.; Dursun, I.; Wang, L. F.; He, Y.; Maculan, G.; Goriely, A.; Wu, T.; Mohammed, O. F.; Bakr, O. M. High-quality bulk hybrid perovskite single crystals within minutes by inverse temperature crystallization. *Nature Communications* **2015,** *6*, 7586.

68. Saidaminov, M. I.; Haque, M. A.; Almutlaq, J.; Sarmah, S.; Miao, X. H.; Begum, R.; Zhumekenov, A. A.; Dursun, I.; Cho, N.; Murali, B.; Mohammed, O. F.; Wu, T.; Bakr, O. M. Inorganic Lead Halide Perovskite Single Crystals: Phase-Selective Low-Temperature Growth, Carrier Transport Properties, and Self-Powered Photodetection. *Advanced Optical Materials* **2017,** *5*, 1600704.

69. Saidaminov, M. I.; Adinolfi, V.; Comin, R.; Abdelhady, A. L.; Peng, W.; Dursun, I.; Yuan, M.; Hoogland, S.; Sargent, E. H.; Bakr, O. M. Planar-integrated single-crystalline perovskite photodetectors. *Nature Communications* **2015,** *6*, 9724.

70. Becker, W.; Hickl, H.; Zander, C.; Drexhage, K. H.; Sauer, M.; Siebert, S.; Wolfrum, J. Time-resolved detection and identification of single analyte molecules in microcapillaries by time-correlated single-photon counting (TCSPC). *Review of Scientific Instruments* **1999,** *70*, 1835-1841.

71. Wahl, M. *Time-Correlated Single Photon Counting*; PicoQuant GmbH: 2017.

72. Dakovski, G. L.; Shan, J. Size dependence of two-photon absorption in semiconductor quantum dots. *Journal of Applied Physics* **2013,** *114*, 014301.

73. de Nalda, R.; del Coso, R.; Requejo-Isidro, J.; Olivares, J.; Suarez-Garcia, A.; Solis, J.; Afonso, C. N. Limits to the determination of the nonlinear refractive index by the Z-scan method. *Journal of the Optical Society of America B-Optical Physics* **2002,** *19*, 289-296.

74. Zhang, Q.; Tian, X. H.; Zhou, H. P.; Wu, J. Y.; Tian, Y. P. Lighting the Way to See Inside Two-Photon Absorption Materials: Structure-Property Relationship and Biological Imaging. *Materials* **2017,** *10*, 223.

75. He, G. S.; Tan, L. S.; Zheng, Q.; Prasad, P. N. Multiphoton absorbing materials: Molecular designs, characterizations, and applications. *Chemical Reviews* **2008,** *108*, 1245-1330.

76. Chen, J. S.; Zidek, K.; Chabera, P.; Liu, D. Z.; Cheng, P. F.; Nuuttila, L.; Al-Marri, M. J.; Lehtivuori, H.; Messing, M. E.; Han, K. L.; Zheng, K. B.; Pullerits, T. Size- and Wavelength-Dependent Two-Photon Absorption Cross-Section of CsPbBr3 Perovskite Quantum Dots. *Journal of Physical Chemistry Letters* **2017,** *8*, 2316-2321.

77. Carrillo-Carrion, C.; Cardenas, S.; Simonet, B. M.; Valcarcel, M. Quantum dots luminescence enhancement due to illumination with UV/Vis light. *Chemical Communications* **2009**, 5214-5226.

78. Peterson, J. J.; Krauss, T. D. Photobrightening and photodarkening in PbS quantum dots. *Physical Chemistry Chemical Physics* **2006,** *8*, 3851-3856.

79. van Sark, W. G. J. H. M.; Frederix, P. L. T. M.; Van den Heuvel, D. J.; Gerritsen, H. C.; Bol, A. A.; van Lingen, J. N. J.; Donega, C. D.; Meijerink, A. Photooxidation and photobleaching of single CdSe/ZnS quantum dots probed by room-temperature time-resolved spectroscopy. *Journal of Physical Chemistry B* **2001,** *105*, 8281-8284.

80. Xi, L. F.; Lek, J. Y.; Liang, Y. N.; Boothroyd, C.; Zhou, W. W.; Yan, Q. Y.; Hu, X.; Chiang, F. B. Y.; Lam, Y. M. Stability studies of CdSe nanocrystals in an aqueous environment. *Nanotechnology* **2011,** *22*, 275706.

81. Aldana, J.; Wang, Y. A.; Peng, X. G. Photochemical instability of CdSe nanocrystals coated by hydrophilic thiols. *Journal of the American Chemical Society* **2001,** *123*, 8844-8850.

82. Tan, Y.; Jin, S.; Hamers, R. J. Influence of Hole-Sequestering Ligands on the Photostability of CdSe Quantum Dots. *Journal of Physical Chemistry C* **2013,** *117*, 313-320.

83. Huang, B.; Xu, R.; Zhang, L.; Yuan, Y.; Lu, C.; Cui, Y.; Zhang, J. Effect of Cu/In ratio and shell thickness on the photo-stability of CuInS2/ZnS nanocrystals. *Journal of Materials Chemistry C* **2017,** *5*, 12151-12156.

84. Cao, Y. M.; Stavrinadis, A.; Lasanta, T.; So, D.; Konstantatos, G. The role of surface passivation for efficient and photostable PbS quantum dot solar cells. *Nature Energy* **2016,** *1*, 16035.

85. Boles, M. A.; Ling, D.; Hyeon, T.; Talapin, D. V. The surface science of nanocrystals. *Nature Materials* **2016,** *15*, 141-153.

86. Krivenkov, V. A.; Samokhvalov, P. S.; Linkov, P.; Prokhorov, S. D.; Martynov, I. L.; Chistyakov, A. A.; Nabiev, I. Effects of surface ligands and solvents on quantum dot photostability under pulsed UV laser irradiation. *Quantum Optics and Quantum Information Transfer and Processing 2015* **2015,** *9505*.

87. Ravi, V. K.; Santra, P. K.; Joshi, N.; Chugh, J.; Singh, S. K.; Rensmo, H.; Ghosh, P.; Nag, A. Origin of the Substitution Mechanism for the Binding of Organic Ligands on the Surface of CsPbBr3 Perovskite Nanocubes. *Journal of Physical Chemistry Letters* **2017,** *8*, 4988-4994.

88. Wu, K.; Liang, G.; Shang, Q.; Ren, Y.; Kong, D.; Lian, T. Ultrafast Interfacial Electron and Hole Transfer from CsPbBr3 Perovskite Quantum Dots. *Journal of the American Chemical Society* **2015,** *137*, 12792-12795.

89. Sheng, X.; Liu, Y.; Wang, Y.; Li, Y.; Wang, X.; Wang, X.; Dai, Z.; Bao, J.; Xu, X. Cesium Lead Halide Perovskite Quantum Dots as a Photoluminescence Probe for Metal Ions. *Advanced Materials* **2017,** *29*, 1700150.

90. Kulbak, M.; Cahen, D.; Hodes, G. How Important Is the Organic Part of Lead Halide Perovskite Photovoltaic Cells? Efficient CsPbBr3 Cells. *Journal of Physical Chemistry Letters* **2015,** *6*, 2452-2456.

91. Niu, G. D.; Guo, X. D.; Wang, L. D. Review of recent progress in chemical stability of perovskite solar cells. *Journal of Materials Chemistry A* **2015,** *3*, 8970-8980.

92. Pan, J.; Sarmah, S. P.; Murali, B.; Dursun, I.; Peng, W.; Parida, M. R.; Liu, J.; Sinatra, L.; Alyami, N.; Zhao, C.; Alarousu, E.; Ng, T. K.; Ooi, B. S.; Bakr, O. M.; Mohammed, O. F. Air-Stable Surface-Passivated Perovskite Quantum Dots for Ultra-Robust, Single- and Two-Photon-Induced Amplified Spontaneous Emission. *Journal of Physical Chemistry Letters* **2015,** *6*, 5027-5033.

93. Akkerman, Q. A.; D'Innocenzo, V.; Accornero, S.; Scarpellini, A.; Petrozza, A.; Prato, M.; Manna, L. Tuning the Optical Properties of Cesium Lead Halide Perovskite Nanocrystals by Anion Exchange Reactions. *Journal of the American Chemical Society* **2015,** *137*, 10276-10281.

94. Koolyk, M.; Amgar, D.; Aharon, S.; Etgar, L. Kinetics of cesium lead halide perovskite nanoparticle growth; focusing and de-focusing of size distribution. *Nanoscale* **2016,** *8*, 6403-6409.

95. Yettapu, G. R.; Talukdar, D.; Sarkar, S.; Swarnkar, A.; Nag, A.; Ghosh, P.; Mandal, P. Terahertz Conductivity within Colloidal CsPbBr3 Perovskite Nanocrystals: Remarkably High Carrier Mobilities and Large Diffusion Lengths. *Nano Letters* **2016,** *16*, 4838-4848.

96. Wang, Y.; Li, X. M.; Zhao, X.; Xiao, L.; Zeng, H. B.; Sun, H. D. Nonlinear Absorption and Low-Threshold Multiphoton Pumped Stimulated Emission from All-Inorganic Perovskite Nanocrystals. *Nano Letters* **2016,** *16*, 448-453.

97. Xu, Y. Q.; Chen, Q.; Zhang, C. F.; Wang, R.; Wu, H.; Zhang, X. Y.; Xing, G. C.; Yu, W. W.; Wang, X. Y.; Zhang, Y.; Xiao, M. Two-Photon-Pumped Perovskite Semiconductor Nanocrystal Lasers. *Journal of the American Chemical Society* **2016,** *138*, 3761-3768.

98. Chen, W.; Bhaumik, S.; Veldhuis, S. A.; Xing, G.; Xu, Q.; Gratzel, M.; Mhaisalkar, S.; Mathews, N.; Sum, T. C. Giant five-photon absorption from multidimensional core-shell halide perovskite colloidal nanocrystals. *Nature Communications* **2017,** *8*, 15198.

99. Wei, K.; Xu, Z. J.; Chen, R. Z.; Zheng, X.; Cheng, X. G.; Jiang, T. Temperature-dependent excitonic photoluminescence excited by two-photon absorption in perovskite CsPbBr3 quantum dots. *Optics Letters* **2016,** *41*, 3821-3824.

100. Han, Q. J.; Wu, W. Z.; Liu, W. L.; Yang, Y. Q. The peak shift and evolution of upconversion luminescence from CsPbBr3 nanocrystals under femtosecond laser excitation. *Rsc Advances* **2017,** *7*, 35757-35764.

101. Contemporary Optoelectronics. Shulika, O.; Sukhoivanov, I., Eds. Springer: 2015; Vol. 199, pp 27-28.

102. Houtepen, A. J.; Hens, Z.; Owen, J. S.; Infante, I. On the Origin of Surface Traps in Colloidal II-VI Semiconductor Nanocrystals. *Chemistry of Materials* **2017,** *29*, 752-761.

103. Dobrovolsky, A.; Sukrittanon, S.; Kuang, Y. J.; Tu, C. W.; Chen, W. M. M.; Buyanova, I. A. Energy Upconversion in GaP/GaNP Core/Shell Nanowires for Enhanced Near-Infrared Light Harvesting. *Small* **2014,** *10*, 4403-4408.

104. Pu, S. C.; Yang, M. J.; Hsu, C. C.; Lai, C. W.; Hsieh, C. C.; Lin, S. H.; Cheng, Y. M.; Chou, P. T. The empirical correlation between size and two-photon absorption cross section of CdSe and CdTe quantum dots. *Small* **2006,** *2*, 1308-1313.

105. Lin, J. H.; Gomez, L.; de Weerd, C.; Fujiwara, Y.; Gregorkiewicz, T.; Suenaga, K. Direct Observation of Band Structure Modifications in Nanocrystals of CsPbBr3 Perovskite. *Nano Letters* **2016,** *16*, 7198-7202.

106. Brennan, M.; Herr, J.; Nguyen-Beck, T.; Zinna, J.; Draguta, S.; Rouvimov, S.; Parkhill, J.; Kuno, M. Origin of the Size-Dependent Stokes Shift in CsPbBr3 Perovskite Nanocrystals. *Journal of the American Ceramic Society* **2017,** *139*, 12201–12208.

107. Li, X. M.; Cao, F.; Yu, D. J.; Chen, J.; Sun, Z. G.; Shen, Y. L.; Zhu, Y.; Wang, L.; Wei, Y.; Wu, Y.; Zeng, H. B. All Inorganic Halide Perovskites Nanosystem: Synthesis, Structural Features, Optical Properties and Optoelectronic Applications. *Small* **2017,** *13*, 1603996.

108. Photodiode Tutorial.

109. Lin, Q. Q.; Armin, A.; Burn, P. L.; Meredith, P. Near infrared photodetectors based on sub-gap absorption in organohalide perovskite single crystals. *Laser & Photonics Reviews* **2016,** *10*, 1047-1053.

110. Walters, G.; Sutherland, B. R.; Hoogland, S.; Shi, D.; Comin, R.; Sellan, D. P.; Bake, O. M.; Sargent, E. H. Two-Photon Absorption in Organometallic Bromide Perovskites. *Acs Nano* **2015,** *9*, 9340-9346.

111. Dou, L. T.; Yang, Y.; You, J. B.; Hong, Z. R.; Chang, W. H.; Li, G.; Yang, Y. Solution-processed hybrid perovskite photodetectors with high detectivity. *Nature Communications* **2014,** *5*, 5404.

112. Konstantatos, G.; Clifford, J.; Levina, L.; Sargent, E. H. Sensitive solution-processed visible-wavelength photodetectors. *Nature Photonics* **2007,** *1*, 531-534.

113. osioptoelectronics. Photodiode Characteristics and Applications. http://www.osioptoelectronics.com/application-notes/an-photodiode-parameters-characteristics.pdf.

114. Directive 2011/65/EU of the European Parliament. http://eur-lex.europa.eu/legal-content/en/TXT/?uri=celex%3A32011L0065.

115. Dipalma, J. R. Bismuth Toxicity. *American Family Physician* **1988,** *38*, 244-246.

116. Leng, M. Y.; Chen, Z. W.; Yang, Y.; Li, Z.; Zeng, K.; Li, K. H.; Niu, G. D.; He, Y. S.; Zhou, Q. C.; Tang, J. Lead-Free, Blue Emitting Bismuth Halide Perovskite Quantum Dots. *Angewandte Chemie-International Edition* **2016,** *55*, 15012-15016.

117. Li, X. M.; Wu, Y.; Zhang, S. L.; Cai, B.; Gu, Y.; Song, J. Z.; Zeng, H. B. CsPbX3 Quantum Dots for Lighting and Displays: Room-Temperature Synthesis, Photoluminescence Superiorities, Underlying Origins and White Light-Emitting Diodes. *Advanced Functional Materials* **2016,** *26*, 2435-2445.

118. Wu, X. X.; Trinh, M. T.; Niesner, D.; Zhu, H. M.; Norman, Z.; Owen, J. S.; Yaffe, O.; Kudisch, B. J.; Zhu, X. Y. Trap States in Lead Iodide Perovskites. *Journal of the American Chemical Society* **2015,** *137*, 2089-2096.

119. Zheng, K. B.; Zidek, K.; Abdellah, M.; Chen, J. S.; Chabera, P.; Zhang, W.; Al-Marri, M. J.; Pullerits, T. High Excitation Intensity Opens a New Trapping Channel in Organic - Inorganic Hybrid Perovskite Nanoparticles. *Acs Energy Letters* **2016,** *1*, 1154-1161.

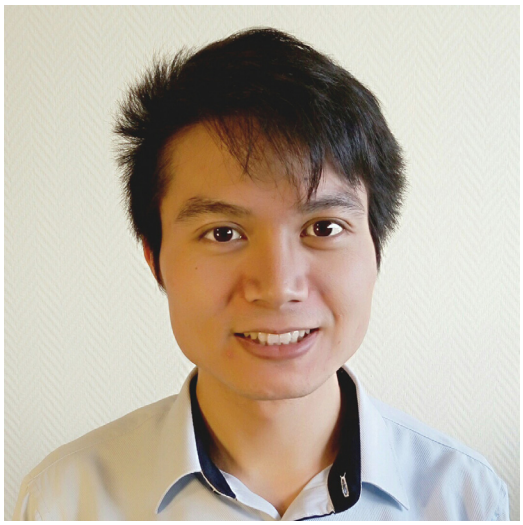

Chemistry makes the world colorful. Certain chemicals emit bright and colorful light. Such compounds are essential for fabricating light emitting devices that are used in our daily life such as LEDs (light emitting diodes), TVs and lasers. Many photophysical processes are involved in the active materials used for fabrication of such devices. A comprehensive understanding of the photophysics of these substances is the key to further improve their performance, optimize manufacturing process and may as well lead to new inventions.

Perovskite is one of the most abundant mineral types on our planet. Perovskite nanocrystals exhibit bright light emission, which makes them suitable as active material for fabricating light emitting devices. This thesis presents the fundamental photophysical processes in perovskite nanocrystals.

Printed by Media-Tryck, Lund 2018 NORDIC SWAN ECOLABEL 3041 0903

LUND UNIVERSITY

ISBN 978-91-7422-567-9

Division of Chemical Physics
Department of Chemistry
Faculty of Science
Lund University

9 789174 225679